

Document downloaded from:

<http://hdl.handle.net/10251/117902>

This paper must be cited as:

Campo García, ADD.; González Sanchís, MDC.; Garcia-Prats, A.; Ceacero Ruiz, CJ.; Lull, C. (2019). The impact of adaptive forest management on water fluxes and growth dynamics in a water-limited low-biomass oak coppice. *Agricultural and Forest Meteorology*. 264:266-282. <https://doi.org/10.1016/j.agrformet.2018.10.016>



The final publication is available at

<https://doi.org/10.1016/j.agrformet.2018.10.016>

Copyright Elsevier

Additional Information

1 **The impact of adaptive forest management on water fluxes and growth dynamics**  
2 **in a water-limited low-biomass oak coppice**

3 Antonio D. del Campo<sup>a\*</sup>, María González-Sanchis<sup>a</sup>, Alberto García-Prats<sup>a</sup>, Carlos J.

4 Ceacero<sup>b</sup>, Cristina Lull<sup>a</sup>

5 a. Research Group in Forest Science and Technology (Re-ForeST), Research Institute of

6 Water and Environmental Engineering (IIAMA), Universitat Politècnica de València,

7 Camí de Vera s/n, E-46022 València (Spain)

8 b. Departamento de Fisiología, Anatomía y Biología Celular, Universidad Pablo de

9 Olavide, E-41013, Sevilla (Spain)

10 \* Corresponding Author: [ancamga@upv.es](mailto:ancamga@upv.es)

11 **Abstract**

12 Marginal semi-arid forests in areas currently affected by climate change are a challenge  
13 to forest management, which has to focus on key functional traits that can effectively  
14 contribute to resistance under extreme drought. We studied the effects of thinning in a  
15 marginal forest by quantifying functional responses relating to growth, carbon and  
16 water fluxes. Two experimental plots were established, one thinned in 2012 and the  
17 other one left as a control. The environmental conditions varied substantially during the  
18 4-year study period, although dry years predominated. There were signs of dieback in  
19 the control with a decreasing inter-annual trend in LAI, as opposed to the treated plots,  
20 where LAI by the end of the study almost reached pre-thinning levels. Sap flow and  
21 transpiration were greatly enhanced by the treatment, with thinned trees transpiring 22.4  
22  $l\ tree^{-1}\ day^{-1}$  in the growing season, about twice the control figures. The seasonal  
23 patterns of transpiration and soil moisture were uncoupled, indicating a contribution of  
24 deep groundwater to the former flux. In the control, limitations to water and carbon  
25 dynamics (canopy conductance) occurred at soil moisture values below 16%, whereas in  
26 the thinned trees these limitations appeared when soil moisture dropped below 10%.  
27 Overall, oaks' transpiration was enhanced with thinning to the point that stand-water  
28 use surpassed that of the control by the second half of the study period, averaging 24%  
29 of gross rainfall in both plots. Soil evaporation increased from 12 to 20% of gross  
30 rainfall after treatment in the overall period. The treatment had a profound watering  
31 effect in this marginal forest, led by fewer trees using the same amount of water as those  
32 in the untreated overstocked plot. This research may provide guidelines for  
33 ecohydrology-oriented silviculture in stands experiencing tree encroachment and  
34 transformation into shrublands that are more prone to global change-induced  
35 disturbances.

36 **Key words:** transpiration, sap-flow, canopy conductance, Shuttleworth–Wallace model,  
37 holm oak, sparse forest.

38 **List of Symbols**

39	$D_B$	Basal diameter (cm)
40	$D_{BH}$	Diameter at breast height (cm)
41	BA	Basal area ( $m^2 ha^{-1}$ )
42	De	Density (trees $ha^{-1}$ )
43	FC	Forest cover (%)
44	Cpa	Crown projected area ( $m^2$ )
45	LAI	Leaf area index ( $m^2 m^{-2}$ )
46	SLA	Specific leaf area ( $cm^2 g^{-1}$ )
47	Pg	Precipitation or gross rainfall (mm)
48	T	Temperature ( $^{\circ}C$ )
49	RH	Relative humidity (%)
50	U	Wind speed ( $m s^{-1}$ )
51	D	Vapour pressure deficit (kPa)
52	$R_{s,a}$	Solar radiation ( $W m^{-2}$ )
53	$R_{n,t}$	Net radiation ( $W m^{-2}$ )
54	$R_{n,f}$	Net radiation over the vegetated area (foliage) ( $W m^{-2}$ )
55	$R_{n,s}$	Net radiation over the bare soil (substrate) ( $W m^{-2}$ )
56	$f$	Fractional vegetation cover (proportion)
57	$\alpha$	Surface albedo (proportion)
58	$R_{l,a,d}$	Downwards long-wave atmospheric radiation ( $W m^{-2}$ )
59	$R_{l,f,u}$	Long-wave upwelling radiation from vegetation ( $W m^{-2}$ )
60	$R_{l,s,u}$	Long-wave upwelling radiation from bare soil ( $W m^{-2}$ )
61	$\sigma$	Stefan-Boltzmann constant ( $5.67 \times 10^{-8} W m^{-2} K^{-4}$ )
62	$\epsilon_a$	Air emissivity
63	$\epsilon_f$	Vegetation emissivity
64	$\epsilon_s$	Bare soil emissivity
65	$T_a$	Air temperature (K)
66	$T_f$	Vegetation temperature (K)
67	$T_s$	Bare soil temperature (K)
68	$\theta$	Soil water content (SWC) ( $m^3 m^{-3}$ )
69	$\theta_{rel}$	Relative soil water content (or relative extractable water, REW) ( $m^3 m^{-3}$ )
70	$\theta_{mx}$	Saturated (maximum) soil water content ( $m^3 m^{-3}$ )
71	$\theta_{mn}$	Minimum soil water content ( $m^3 m^{-3}$ )
72	$\theta_{fc}$	Field capacity ( $m^3 m^{-3}$ )
73	$v_s$	Sap flow velocity ( $cm h^{-1}$ )
74	Sa	Sapwood area ( $cm^2$ )
75	$S_f$	Sap flow ( $l tree^{-1} hour^{-1}$ )
76	ET	Evapotranspiration (mm)
77	$E_t$	Stand transpiration (mm)
78	$E_s$	Evaporation from soil (mm)
79	$E_r$	Residual evapotranspiration (mm)
80	$E_i$	Interception or wet canopy evaporation (mm)
81	$G_s$	Canopy conductance ( $mm s^{-1}$ )
82	$\Omega$	Decoupling coefficient
83	$\gamma$	Psychrometric constant ( $kPa K^{-1}$ )

84	$\Delta$	Slope of the saturated vapor pressure curve (kPa K <sup>-1</sup> )
85	$\varepsilon$	Ratio of $\Delta$ to $\gamma$
86	$g_a$	Aerodynamic conductance (m s <sup>-1</sup> )
87	$z_h$	Mean canopy height (m)
88	$z_r$	Reference height (m)
89	$z_0$	Vegetation surface roughness length (m)
90	$d$	Zero-plane displacement of vegetated surfaces (m)
91	$k$	von Kármán's constant (dimensionless)
92	$m$	Slope or stomatal sensitivity to D
93	$G_{sref}$	Reference canopy conductance at D=1 kPa,
94	$\lambda ET$	Latent heat flux from the complete canopy (W m <sup>-2</sup> )
95	$\lambda E_t$	Latent heat flux from foliage (W m <sup>-2</sup> )
96	$\lambda E_s$	Latent heat flux from substrate (W m <sup>-2</sup> )
97	$A_f$	Available energy at the foliage (W m <sup>-2</sup> )
98	$A_s$	Available energy at the substrate (W m <sup>-2</sup> )
99	$c_p$	Specific heat of air at constant pressure (J kg <sup>-1</sup> K <sup>-1</sup> )
100	$D_m$	Vapor pressure deficit at canopy source height (kPa)
101	$\rho$	Air density (kg m <sup>-3</sup> )
102	$n$	Parameter with value of 2 for hypostomatous leaves
103	$r_a$	Aerodynamic resistance above the canopy (s m <sup>-1</sup> )
104	$r_{a,f,h}$	Bulk boundary-layer resistance of the foliage for sensible heat (s m <sup>-1</sup> )
105	$r_{a,l}$	Leaf boundary-layer resistance for sensible heat and water vapour (s m <sup>-1</sup> )
106	$r_{a,s}$	Aerodynamic resistance between the substrate (s m <sup>-1</sup> )
107	$r_{s,f}$	Bulk stomatal resistance of the foliage (s m <sup>-1</sup> )
108	$r_{s,s}$	Substrate (soil and mulch) resistance to evaporation (s m <sup>-1</sup> )
109	$r_s$	Soil layer surface resistance (s m <sup>-1</sup> )
110	$r_m$	Extraneous mulch resistance (s m <sup>-1</sup> )
111	$r_d$	Diffusive component of the vapor transport resistance (s m <sup>-1</sup> )
112	$h_m$	Thickness of the mulch (m)
113	$D_{eff}$	Effective diffusivity of water vapor in the porous medium (m <sup>2</sup> s <sup>-1</sup> )
114		
115		

## 116 **1. Introduction**

117 Mediterranean forests, a particular case of semi-arid forests, suffer from a combination  
118 of stressors that trigger tree mortality (Allen et al., 2010; García de la Serrana, 2015;  
119 Doblas-Miranda et al., 2017) and require urgently proactive-adaptive silviculture  
120 (Lindner et al., 2014). Holm oak (*Quercus ilex* L.) is one of the most important forest  
121 species in the western Mediterranean basin, covering about 5.4 Mha, more than half of  
122 which are in Spain (Terradas, 1999; Ruiz de la Torre, 2006). While at the northern edge  
123 of its distribution range, the species is colonizing new areas (Delzon et al., 2013), in  
124 Mediterranean Spain holm oak forests have shown climate-related mortality and growth

125 decline since the last century (Barbeta and Peñuelas, 2016; Camarero et al., 2016;  
126 Peñuelas et al., 2017; Gentilesca et al., 2017). In fact, observed trends in climate may  
127 push marginal populations of holm oak close to their distributional limit (Terradas and  
128 Savè, 1992; Martinez-Vilalta et al., 2003; Peñuelas et al., 2017). Following a decreasing  
129 precipitation gradient, holm oak forests become scarcer towards south-eastern Spain  
130 where they can be found growing on highlands and mountains with less xeric conditions  
131 (Terradas and Savè, 1992; Ruiz de la Torre, 2006). These scattered forests can be  
132 considered as the rear edge of the species' distribution (Hampe and Petit, 2005) and  
133 may have a comparably different ecophysiological response to drought stress (Gratani et  
134 al., 2003; Valero-Galván et al., 2011). In this sense, these remnant populations are of  
135 critical importance in a global change context, not only from a conservation and  
136 management perspective, but also for the deployment of climate-adjusted or admixture  
137 provenancing strategies elsewhere in assisted migration programs (Prober et al., 2015).  
138 The management implications of either ongoing-declining or prone-to-decline oak  
139 stands have received attention from the research community, seeking appropriate  
140 measures for improving the resilience and resistance of forests (Mayor and Rodà, 1993;  
141 Gracia et al., 1999; López et al., 2003; Moreno and Cubera, 2008; Limousin et al., 2008,  
142 2009; Cotillas et al., 2009; Gea-Izquierdo et al., 2009; Gentilesca et al., 2017; Cabon et  
143 al., 2018). In these studies, selective thinning was studied as an adaptive measure to  
144 compensate for rainfall reduction and, in corroboration of studies of other species and  
145 forest-types (Bréda et al., 1995), they report enhanced tree growth and climate-growth  
146 relationships, increased soil water content, higher tree-water use and reduced stand  
147 transpiration after thinning.  
148 However, the structural characteristics of the oak stands found across the distribution  
149 range of the species as well as their site conditions are very different, just as their

150 potential responses to extreme droughts are (Barbeta and Peñuelas, 2016), so that the  
151 specific targets/effects of thinning may vary. Some researchers (Moreno and Cubera,  
152 2008; Cotillas et al., 2009; Gea-Izquierdo et al., 2009) have studied open holm oak  
153 woodlands (silvopastoral systems), where tree density and competition are low (usually  
154 fewer than 200 trees ha<sup>-1</sup>) and tree structure is relatively homogeneous (tall trees with  
155 large basal areas). On the other hand, most studies of thinning (carried out in north-  
156 eastern Spain and southern France) have examined dense multi-stemmed coppices of  
157 *Quercus ilex* subsp. *ilex* (LAI ~ 2.0 - 4.0 m<sup>2</sup> m<sup>-2</sup>) that result from historical harvesting  
158 for charcoal (López et al., 2003), with contrasting responses appearing between trees of  
159 different crown classes (Galiano et al., 2012; Olivar et al., 2014). Structurally, thinning  
160 reduces stand density, decreases competition and increases the availability of resources  
161 (light, water, nutrients) for the remaining trees (Bréda et al., 1995), thus promoting  
162 functional changes as long as the increased availability remains significant (Limousin et  
163 al., 2009; Cabon et al., 2018). The sequence of functional responses to drought in holm  
164 oak on different timescales has been extensively studied and was recently compiled by  
165 Barbeta and Peñuelas (2016). Responses related to carbon and water cycles, phenology  
166 and growth are the key traits in this regard. A focus on maintaining and/or enhancing  
167 these ecological processes and functional characteristics, rather than specific structures  
168 and species composition, must guide forest treatments designed to enhance resilience  
169 (Seidl et al., 2016). This function-to-structure approach can identify those structure  
170 assemblages that are less prone to drought-induced decline and that could benefit more  
171 from management practices, thus optimizing the limited budgets and practical decision-  
172 making. Targeting functional traits must be related to a species' drought tolerance and  
173 resource use strategy and must respond positively to stand density reduction, such as  
174 growth, leaf traits (specific leaf area, SLA) (Cotillas et al., 2009; Gea-Izquierdo et al.,

175 2009; Stahl et al., 2014), canopy conductance ( $G_s$ ) and its variations with both soil  
176 moisture ( $\theta$ ) and atmospheric demand for water (D) (Novick et al., 2016; Grossiord et  
177 al., 2017), tree transpiration and evapotranspiration (ET) components at the stand scale,  
178 etc. (Grant et al., 2013; Klein et al., 2013; del Campo et al., 2014).

179 Unfortunately, adaptive management in low-biomass shrublands has received much less  
180 attention, as most studies have been conducted in core or central habitats of the species,  
181 where dry years are more the exception than the rule. Following the approach explained  
182 above, the aim of this study is to evaluate the effects of selective thinning and shrub  
183 clearance in a marginal low-biomass forest of Holm oak by examining the response to  
184 selected functional traits related to carbon and water cycles over an inter-annual span  
185 (Barbeta and Peñuelas, 2016). The specific objectives are to study the effect of the  
186 treatment i) on growth and leaf traits in the years following thinning, ii) on sap flow and  
187 the response of transpiration to environmental variables, iii) on  $G_s$  as a proxy for the  
188 trade-offs between carbon and water fluxes at the stand scale and iv) on the stand ET  
189 and its components (transpiration and soil evaporation).

190 We hypothesize that thinning will increase water availability for the remaining trees,  
191 triggering eco-physiological responses that will improve drought resistance at the tree  
192 level whilst decreasing stand water-use. We expect these effects to last during the four  
193 years studied (short-term effect).

## 194 **2. Materials and Methods**

### 195 *2.1. Study site and experimental trial*

196 The study was carried out in a marginal oak forest located in the southwest region of  
197 Valencia province in Spain (39°04'-N, 1°14'-W elevation 1,080-1,100 m a.s.l.). The  
198 average annual rainfall in a meteorological station located nearby at 900 m a.s.l. is 466  
199 mm. This rainfall typically shows high intra- and inter-annual variability with seasonal

200 and annual coefficients of variation of 52 and 28%, respectively (Perez-Cueva, 1994).  
201 Mean annual temperature is 12.8°C, and the mean annual potential evapotranspiration is  
202 749 mm (Thornthwaite, 1948). The soil is relatively shallow (10-40 cm), sandy-silty-  
203 loam textured (44% sand; 33% silt; 23% clay, on the top 10 cm; below that depth, sand:  
204 52%; silt: 28; clay: 20%) and basic pH (8.0±0.1). Additional properties of soils are  
205 described in di Prima et al. (2017). Parent rock is a karstified limestone that gives rise to  
206 rocky soils with volumetric content of stones and rocks that ranges between 48 and  
207 69%, depending on depth. Boreholes in the plots (up to 4 meters deep) revealed a high  
208 degree of rock fissuring that provides reservoirs of deep water.

209 The dominant species at the study site is Holm oak (*Quercus ilex* subsp. *ballota* (Desf.)  
210 Samp.) and accompanying species are *Q. faginea* Lam., *Pinus halepensis* Mill.,  
211 *Juniperus phoenicea* L. and *J. oxycedrus* L. This coppice oak forest is the result of  
212 traditional fuelwood harvesting that fell into disuse in the 1970's, has high stem  
213 densities (Table 1) and, accordingly, high intraspecific competition that might be  
214 responsible for the dieback observed after severe dry years. The forest has low biomass,  
215 with aboveground values of 49.7 Mg/ha (23.1 Mg C/ha) calculated from site/species-  
216 specific allometric equations developed at the time of thinning (see below): Biomass  
217 (kg) = 1.08 \*  $D_{BH}^2$  (cm) - 16.4 \*  $D_{BH}$  (cm) + 68.67, with  $D_{BH} > 7$  cm,  $r^2=0.95$ ). There  
218 has been no forest management, as this is marginal and protective forest. Site conditions  
219 are harsh (soil and recurrent droughts (Fernandes et al., 2016)) and symptoms of decay,  
220 such as top-tree death, foliage loss, death of interspersed *Q. faginea* trees and increasing  
221 frequency of pine saplings, can be observed inside the experimental plots.

222 This study is part of a broader study where water and nutrient cycles and soil properties  
223 are monitored for an integrated assessment of the ecohydrology of the ecosystem. In  
224 May 2012, experimental thinning (and shrub clearance) took place in a rectangular plot

225 (T), slope 31%, NW aspect, of about 1,800 m<sup>2</sup>, split into three replicates or blocks of  
226 similar size, leaving about one third of the initial standing trees (about 315 trees/ha)  
227 (Table 1). A run-off collecting trench at the lower boundary of the slope forced us to  
228 site the three blocks consecutively from upslope to downslope (no randomized layout).  
229 Adjoining the thinned area, a control plot (C) of similar size was established and also  
230 split into three blocks. The thinning/clearance removed most of the shrubs, the trees  
231 with smaller diameters and multi-stemmed trees (leaving only the bigger stem). The  
232 thinning aimed to achieve relatively homogeneous tree distribution, based on forest  
233 cover. Thinning was conducted and supervised by the Forest Service of Valencia;  
234 timber and coarse woody debris were removed outside the plots, whereas fine woody  
235 debris was piled and grinded into mulch on the plots. Climate, parent material (soil  
236 origin), topography and biota were considered as the constant in both plots, whereas  
237 forest management (thinning treatment) was taken as the factor.

## 238 *2.2. Forest structure and tree growth measurement*

239 Forest structure within the plots was characterized in May 2012 and at the end of the  
240 study period in November 2016, recording the following variables: diameter at basal  
241 and breast heights ( $D_B$ , and  $D_{BH}$  respectively, cm), basal area ( $BA$ , m<sup>2</sup> ha<sup>-1</sup>) and density  
242 ( $De$ , trees ha<sup>-1</sup>). Measuring tree diameters and counting all trees in the plots calculated  
243  $BA$  and  $De$ . Diameter distribution was classified into 4 classes:  $D_{BH} \leq 7.5$  (DC1),  
244  $7.5 < D_{BH} \leq 11$  (DC2),  $11 < D_{BH} \leq 15$  (DC3),  $D_{BH} > 15$  (DC4) (figures in cm). Forest cover  
245 ( $FC$ , %) was determined just once in October 2015, with a vertical densitometer (GRS,  
246 Arcata, CA, USA) with 50 readings per block taken above 1.7 m in a 3x3 m grid, giving  
247 a value of  $39.3 \pm 3.4$  and  $62.7 \pm 1.9\%$  for the treated and control plots, respectively (shrubs  
248 below that height make total ground cover higher). All measurements were made in  
249 areas at least 2 m away from the plot limits to avoid edge effects. Crown projected area

250 ( $C_{pa}$ ,  $m^2$ ) was calculated by averaging the measurements of 8-10 orthogonal crown  
251 diameter projections in 9-12 trees per treatment. Leaf Area Index (LAI,  $m^2 m^{-2}$ ) was  
252 measured once per season in each block by a LAI-2000 sensor (LI-Cor, 1991, LI-Cor  
253 Inc., Lincoln, NE, USA) under direct solar radiation, as described in Molina and del  
254 Campo (2011) and Leblanc and Chen (2001). Average measured values were  $0.61 \pm 0.07$   
255 and  $1.13 \pm 0.22 m^2 m^{-2}$  for the treated and control plots, respectively. Inadequate  
256 atmospheric conditions led to defective readings and gaps that were corrected and filled  
257 with estimations from the level-4 MODIS global Leaf Area Index satellite product  
258 (NASA, LPDAAC) in order to complete the seasonal series. The product is composited  
259 every 8 days (monthly averages were performed) at 1-kilometer resolution on a  
260 sinusoidal grid. For the coverage of the study site, the h17v05 tile is required, where h  
261 and v denote the horizontal and vertical tile number, respectively. The MODIS LAI  
262 dataset provided in Hierarchical Data Format (HDF) was imported to GeoTIFF format  
263 by MODIS Reprojection Tool (MRT) (NASA) and reprojected from the Integerized  
264 Sinusoidal (ISIN) projection to the UTM projection system.

265 Growth and leaf traits were measured at the end of each year in 16-21 trees per plot  
266 proportionally distributed across diameter classes and blocks, adapting the basic concepts  
267 and methodology for oaks from Girard et al. (2011). In each surveyed tree, six dominant  
268 branches were selected in the upper half of the crown, distributed on both north and  
269 south aspects. Then, the shoots of the last growing season were identified and counted for  
270 each branch. A sample of 10-15 shoots of the annual growth per tree were measured in  
271 the following metrics: shoot length (cm), basal diameter of the shoot (mm), number of  
272 growth cycles (in case there was more than one), number of leaves of the shoot, total leaf  
273 area of the shoot (measuring maximum width and length of individual leaves and  
274 computing the area of the oval,  $cm^2$ ), and specific leaf area (SLA,  $cm^2 g^{-1}$ ). This assay

275 was also done for the epicormic shoots and resprouts in the treated plot in the last year's  
276 growth (2016), as this growth became very apparent from 2015 on. Finally, for a  
277 calculation of tree-based LAI, an independent set of LAI was measured in November  
278 2016 under the crown in a subsample of 18 trees (9 per treatment, three per block)  
279 belonging to the four diametric classes. For each tree, a set of A-type (same clearing as  
280 in the measurements for the LAI plot) and B-type (front, right and left sides of the trunk  
281 at 1.0 m above ground) measurements were taken.

### 282 *2.3. Environmental variables and field instrumentation*

283 This study spans the period from October 1, 2012 to December 30, 2016. As the  
284 thinning treatment took place in May 2012, we considered it appropriate to provide  
285 values in the first year of the treatment even though that year was monitored only in its  
286 last quarter. Precipitation or gross rainfall ( $P_g$ ) was continuously measured by means of  
287 a tipping-bucket rain gauge located in an open area apart from the experimental plots  
288 with 0.2-mm resolution (7852, Davis Instruments Corp., Hayward, CA, USA),  
289 programmed to measure at 10-min intervals and connected to a CR1000 data-logger  
290 (Campbell Sci., UT, USA). Gaps were filled in with records from a standard rain gauge  
291 station located 1.5 km away with a daily timescale (Ayora-La Hunde SAIH network).  
292 Air temperature ( $T$ , °C) and relative humidity (RH, %) were measured inside the  
293 experimental plots (2 m above ground) and above the canopy (6.5 m above ground) in  
294 the buffer zone between both plots. The sensors (RH/T sensor, Decagon Devices,  
295 Pullman, WA, USA) were connected to EM50 (Decagon) dataloggers and programmed  
296 to measure at 10-min intervals. Wind speed ( $U$ ,  $\text{m s}^{-1}$ , 7911 anemometer, Davis  
297 Instruments Corp.) and solar radiation ( $R_{s,a}$ ,  $\text{W m}^{-2}$ , Campbell CS300 pyranometer,  
298 Campbell Sci., Logan, UT, USA) were measured above the canopy (6.5 m) on the same  
299 RH/T mast and recorded on the CR1000. Temperature and RH data were subsequently

300 used to obtain values for the vapor pressure deficit (D, kPa). In line with the two-layer  
 301 approach for ET calculation (see below), net radiation ( $R_{n,t}$ ) was estimated as in  
 302 Domingo et al. (2000):

$$303 \quad R_{n,t} = fR_{n,f} + (1 - f) R_{n,s} = R_{s,a}(1 - \alpha) + R_{l,a,d} - fR_{l,f,u} - (1 - f)R_{l,s,u} \quad (1)$$

304 where  $R_{n,f}$  and  $R_{n,s}$  are the net radiation terms ( $\text{W m}^{-2}$ ) over the vegetated area (foliage)  
 305 and over the bare soil (substrate), respectively. The term  $f$  is the fractional vegetation  
 306 cover (total cover, not just trees; C: 0.769; T: 0.393 until summer 2014, and  
 307 exponentially growing up to 0.569 in summer 2016). The term  $\alpha$  is the surface albedo,  
 308 calculated for C and T plots by using Landsat 8 OLI/TIRS Data (30x30 m resolution)  
 309 and following the Surface Energy Balance Algorithm for Land (SEBAL; Bastiaanssen  
 310 et al., 1998). The term  $R_{l,a,d}$ , is the downwards long-wave atmospheric radiation and  
 311  $R_{l,f,u}$  and  $R_{l,s,u}$  are the long-wave upwelling radiation from vegetation and bare soil,  
 312 respectively. These were calculated as:

$$313 \quad R_{l,a,d} = \sigma \varepsilon_a T_a^4 \quad (2)$$

$$314 \quad R_{l,f,u} = \sigma \varepsilon_f T_f^4 \quad (3)$$

$$315 \quad R_{l,s,u} = \sigma \varepsilon_s T_s^4 \quad (4)$$

316 With  $\sigma$  the Stefan-Boltzmann constant ( $5.67 \times 10^{-8} \text{ W m}^{-2} \text{ K}^{-4}$ ),  $\varepsilon_a$ ,  $\varepsilon_f$  and  $\varepsilon_s$  are the air,  
 317 vegetation and bare soil emissivity, respectively, and  $T_a$ ,  $T_f$  and  $T_s$  are the air, vegetation  
 318 and bare soil temperatures (K), respectively. Soil temperature at 1 cm depth was linearly  
 319 inferred from readings at 5 and 15 cm depth (see below);  $\varepsilon_f$  and  $\varepsilon_s$  were set to 0.985 and  
 320 0.986, respectively (Rubio et al., 1997); and  $\varepsilon_a$  was calculated as proposed by Idso  
 321 (1981).

322 Soil water content (SWC,  $\theta$ ,  $\text{m}^3 \text{ m}^{-3}$ ) was continuously measured for the whole period  
 323 every 10 minutes by means of FDR probes (5TE and EC-5, Decagon Devices Inc.,  
 324 Pullman, WA, USA) connected to the CR1000 data-logger. Sensors were installed by

325 digging three pits per block (9 per plot and 18 total) along contour lines. In the central  
326 pit of each block, three sensors (5TE, which also provide soil temperature) were  
327 inserted horizontally at depths of 5, 15 and 30 cm into the unaltered upslope pit face,  
328 whereas in the other two pits in the block, only one sensor (EC-5) was inserted at 15 cm  
329 depth. Total sample size per plot (treated/control) was 15 sensors in the 9 spots. After  
330 installation, the pits were backfilled with the excavated soils and slightly compacted up  
331 to similar bulk density to that of unaltered soil. Thus, sensor readings include the effect  
332 of stoniness in the pit (as rocks do not hold moisture). Calibrations were discarded as  
333 the observed increase in  $\theta$  after calibrating was offset when taking into account the  
334 stoniness effect in field conditions (which we did not want to obviate), and because of  
335 the temporal drifts observed in several cases. Thus, we used default calibration (for  
336 mineral soils) in all cases after observing that the use of relative variables rather than  
337 absolute  $\theta$  would minimize the impact of any changes from the calibration curve on the  
338 patterns of  $\theta$  fluctuations (Detty and McGuire, 2010). The relative  $\theta$  (or relative  
339 extractable water, REW) was computed for the 10-min  $\theta$  values as:

$$340 \quad \theta_{rel} = \frac{\theta - \theta_{mn}}{\theta_{mx} - \theta_{mn}} \quad (5)$$

341 where  $\theta_{mx}$  and  $\theta_{mn}$  are the saturated (maximum) and minimum soil water content of the  
342 probe. The range of  $\theta$  for each probe was computed as the extreme values that the  
343 sensor recorded during the entire monitoring period. Field capacity for each probe was  
344 calculated from the steady values of  $\theta$  following gentle rainfall events with at least 20  
345 mm ( $\theta_{fc}$ ). Averaged soil water content at field capacity was 0.19 and 0.20  $\text{m}^3 \text{m}^{-3}$  for C  
346 and T, respectively;  $\theta_{mx}$  and  $\theta_{mn}$  averaged, respectively, 0.33 and 0.02  $\text{m}^3 \text{m}^{-3}$  in both  
347 plots.

#### 348 *2.4 Sap flow and Transpiration*

349 Sap flow velocity ( $v_s$ ,  $\text{cm h}^{-1}$ ) was measured hourly through the Heat Ratio Method,  
350 HRM (Burgess et al., 2001) by 14 sap flow sensors powered by a 12 V battery  
351 connected to a solar panel and a data-logger (Smart Logger, ICT International,  
352 Armidale, NSW, Australia). Sensors were installed on the upslope side of the trunk at a  
353 variable height depending on the trunk's shape (at between 0.3 and 1.0 m height). Each  
354 sensor has a heater between two needles containing two thermocouples each, located  
355 27.5 mm and 12.5 mm from their bases. The sensors were distributed in both plots  
356 proportionally to the different diameter classes. This sample size falls within the range  
357 normally considered in tree water-relations studies (Granier, 1987; Klein et al., 2013;  
358 Martínez-Vilalta et al., 2003).

359 Sapwood area ( $S_a$ ,  $\text{cm}^2$ ) was at first calculated by subtracting heartwood area from the  
360 inner-bark area in a sample of cores and slices obtained when applying the treatments.  
361 However, we discarded this method due to its high subjectivity and lack of direct  
362 sapwood data from the sampled trees. Instead, we opted for a linear fit of  $v_s$  from both  
363 thermocouples at both depths to obtain the depth at which  $v_s$  equals 0 (del Campo et al.,  
364 2014). This linear approach is expected to slightly underestimate the innermost  $S_a$ ,  
365 which usually has very low sap flux values (Berdanier et al., 2016).  $S_a$  was divided into  
366 three different sections to assign different  $v_s$  values and consequently to calculate hourly  
367 and daily values of sap flow ( $S_f$ ,  $\text{l tree}^{-1} \text{ hour}^{-1}$ ) (Hatton et al., 1990; Delzon et al., 2004)  
368 as follows: 1) the  $v_s$  from the outer thermocouple was assigned to the  $S_a$  from the  
369 cambium to the mid-point between the outer and inner thermocouples (i.e. 20 mm  
370 depth); (2) the  $v_s$  from the inner thermocouple was assigned to the  $S_a$  from 20 mm to  
371 the depth of the probe (35 mm depth from the cambium); and (3)  $0.5v_s$  from the inner  
372 thermocouple was assigned to the remaining area from 35 mm deep to the beginning of  
373 the heartwood or to the pith (if heartwood was not present). Up-scaling  $S_f$  ( $\text{l tree}^{-1}$ ) to

374 stand transpiration per plot ( $E_t$ , mm,  $l\ m^{-2}$ ) used the number of trees ( $De$ , tree  $m^{-2}$ ) as  
375 scalar. We obtained a correction factor ( $cf$ ) by regressing  $S_f$  on  $S_a$  ( $r^2 > 91\%$ ) so that the  
376  $S_f$  corresponding to the mean sampled tree was corrected to the mean plot tree.

377 Accordingly,  $E_t$  per plot was calculated as:

$$378 \quad E_t = S_f De cf \quad (6)$$

379 Data were quality-controlled for any possible spikes and gaps. In some cases,  $v_s$  flow  
380 data were lost for more than 15-day spells, because of datalogger/sensor malfunction,  
381 battery failure and/or rodents' activity. In these cases, an Artificial Neural Network  
382 model was used to estimate  $E_t$ , as described in Fernandes et al. (2015).

### 383 *2.5. Canopy conductance ( $G_s$ )*

384  $G_s$  ( $mm\ s^{-1}$ ) is an essential parameter that represents the physiological control of  
385 transpiration by environmental variations, and thus regulates tree-water use and carbon  
386 uptake (Novick et al., 2016; Grossiord et al., 2017).  $G_s$  is usually calculated from sap  
387 flow measurements by means of the reverse form of the Penman-Monteith equation  
388 (Granier and Breda, 1996). Due to the sparseness of the trees,  $G_s$  was calculated in a  
389 similar way, but including the sparse canopy and using the Shuttleworth and Wallace  
390 (1985) physical model as detailed in Lhomme et al. (2012). Thus,  $G_s$  derived in this way  
391 reflects contributions only from stomatal conductance and not from the whole surface.  
392 Climate data above the canopy (6.5 m) were used in the model (see point 2.6 ET  
393 partitioning). Periods when  $R_{s,a}$  was lower than  $400\ W\ m^{-2}$  and sap flow ( $v_s$ ) was close  
394 to zero were eliminated in order to decrease relative inaccuracy in  $G_s$  calculation  
395 (Granier et al., 2000). A threshold of  $D$  was taken as  $0.6\ kPa$  to remove the wettest air  
396 conditions when errors in  $G_s$  estimates are higher than 10% (Ewers and Oren, 2000).  
397 We assumed negligible stem capacitance and no time lag between transpiration and soil  
398 water uptake for this subspecies (Trifilò et al., 2015). The threshold for  $R_{s,a}$  adopted

399 here minimizes a possible capacitance effect of the trees, as previously observed  
 400 (Lhomme et al. 2001). In any case, the condition of high aerodynamic coupling between  
 401 the air inside the canopy and the air from the bulk atmosphere was tested by calculating  
 402 the decoupling coefficient  $\Omega$  (Jarvis and McNaughton, 1986) that ranges between 0 and  
 403 1, with 0 representing full stomatal control of  $E_t$  (highly coupled):

$$404 \quad \Omega = \frac{(\varepsilon + 1)}{\left(\varepsilon + 1 + \frac{g_a}{G_s}\right)} \quad (7)$$

405 where  $\varepsilon$  is the ratio of the slope of the relationship between saturation vapor pressure  
 406 and temperature ( $\Delta$ ) to the psychrometric constant ( $\gamma$ );  $g_a$  is the aerodynamic  
 407 conductance ( $\text{m s}^{-1}$ ) above the canopy calculated for neutral conditions as:

$$408 \quad g_a = \frac{k^2 U}{\ln^2 \left[ \frac{(z_r - d)}{z_0} \right]} \quad (8)$$

409 expressed as a function of wind speed;  $z_0$  is vegetation surface roughness length and  $d$  is  
 410 the zero-plane displacement of vegetated surfaces, both calculated according to Shaw  
 411 and Pereira (1982) as functions of mean canopy height (dominant and co-dominant  
 412 trees,  $z_h = 5.20$  and  $5.78$  m for C and T, respectively) and LAI (mean LAI = 1.13 and  
 413 0.61 for C and T);  $d_{\text{C}} = 3.32$ ;  $d_{\text{T}} = 3.29$ ;  $z_{0\text{C}} = 0.624$ ;  $z_{0\text{T}} = 0.642$ . The term  $k$  is the von  
 414 Kármán constant (0.41) and  $U$  ( $\text{m s}^{-1}$ ) is the wind speed at reference height  $z_r$  (6.5 m).  
 415  $G_s$  is affected by  $\theta$  and  $D$ : decreasing  $\theta$  limits the movement of water to evaporating  
 416 stomata and reduces  $G_s$ ; and increasing  $D$  causes stomata closure, thus affecting  $G_s$  in an  
 417 independent fashion (Novick et al., 2016). Disentangling the impact of these two drivers  
 418 is important as  $\theta$  and  $D$  are decoupled at short temporal scales and the effects of  
 419 thinning on the magnitude of carbon and water fluxes may become less effective  
 420 (Novick et al., 2016). To calculate  $G_s$  sensitivity to  $D$ , we used (Granier et al., 1996):

$$421 \quad G_s = -m \ln(D) + G_{sref} \quad (9)$$

422 where  $G_s$  is an estimate of average stomatal conductance over the canopy ( $\text{mm s}^{-1}$ ),  $-m$   
423 is the slope or stomatal sensitivity to  $D$  ( $-dG_s/d\ln(D)$ ) and  $G_{sref}$  is the reference canopy  
424 conductance at  $D=1$  kPa and can be used as surrogate for  $G_{smax}$  (Chen et al., 2014). The  
425 analysis sorted the  $G_s$  data set into 4 categories of  $\theta_{rel}$  ( $\theta_{rel}\leq 0.2$ ;  $0.2<\theta_{rel}\leq 0.4$ ;  
426  $0.4<\theta_{rel}\leq 0.6$ ;  $\theta_{rel}>0.6$ ). A boundary line analysis on  $G_s$  versus  $D$  within each category  
427 was carried out (Erwens et al., 2005; Chen et al., 2014). The term  $G_s$  is also sensitive to  
428 variations in  $R_{s,a}$  and  $T$ . However, we filtered for  $R_{s,a}>400$   $\text{W m}^{-2}$ . Variations in diurnal  
429  $G_s$  can often be explained mostly by  $D$ , which correlates directly with  $R_{s,a}$  and  $T$ , so that  
430 neglect of these dependencies does not bias the analysis (Novick et al., 2016). In each  
431 category of  $\theta_{rel}$ ,  $G_s$  was further partitioned into 0.2 kPa  $D$  intervals and the mean and  
432 standard deviation of  $G_s$  within each interval were calculated. The outliers were  
433 removed ( $p<0.05$ , Dixon's test) and the data above the mean and one standard deviation  
434 of  $G_s$  were selected (Ewers et al., 2005). The parameters of equation 9 can then be  
435 related to the categorizing variables ( $D$  and  $\theta$ ). This boundary analysis provides the best  
436 estimate of physiological response because the boundary line occurs during conditions  
437 that lead to the highest  $G_s$  at any given  $D$  (Ewers et al., 2005).  $G_{sref}$  accounts for the  
438 effects of soil water on  $G_s$  whereas  $-m$  describes the effects of  $D$  on  $G_s$ . The ratio of  $-m$   
439 to  $G_{sref}$  is 0.6 across a wide range of species and environments (Oren et al., 1999), with  
440 lower values than 0.6 when trees show less strict regulation of the leaf water potential  
441 (allowing the minimum leaf water potential to drop with increasing  $D$ ) or the range of  $D$   
442 broadens so that the slope decreases; and higher than 0.6 when the ratio of boundary  
443 layer conductance to stomatal conductance is low (Oren et al., 1999).

#### 444 2.6. *ET partitioning*

445 The low values of both LAI and FC at our experimental site indicate that this cannot be  
446 considered as dense vegetated canopy, especially in the treated plot. This, together with

447 the need to distinguish between soil evaporation and transpiration, made it advisable to  
 448 use the Shuttleworth and Wallace (1985) two-layer model to calculate soil evaporation  
 449 separately. The Shuttleworth–Wallace (S–W) model assumes that the evaporation from  
 450 a stand of sparse vegetation consists of fluxes from the upper canopy (main foliage) and  
 451 the substrate (which may be bare soil or grass). Although the Penman–Monteith one-  
 452 layer model (Monteith and Unsworth, 1990) has been widely used and tested, it may be  
 453 inappropriate for sparsely vegetated canopies (Zhang et al., 2008). In the two-layer S-W  
 454 model, the latent heat flux from the complete canopy ( $\lambda ET$ ) is expressed as the simple  
 455 sum of two components:  $\lambda E_t$  (latent heat flux from foliage) and  $\lambda E_s$  (latent heat flux  
 456 from substrate; substrate is defined here as the non-vegetated area) (Lhomme et al.,  
 457 2012):

$$458 \quad \lambda E_t = \left( \frac{\Delta A_f + \rho C_p \frac{D_m}{r_{a,f,h}}}{\Delta + \gamma \left( n + \frac{r_{s,f}}{r_{a,f,h}} \right)} \right) \quad (10)$$

$$459 \quad \lambda E_s = \left( \frac{\Delta A_s + \rho C_p \frac{D_m}{r_{a,s}}}{\Delta + \gamma \left( 1 + \frac{r_{s,s}}{r_{a,s}} \right)} \right) \quad (11)$$

460 where  $A_f$  and  $A_s$ , are the available energy at the foliage and substrate, respectively ( $W$   
 461  $m^{-2}$ ), calculated according to eq. (1) as in Domingo et al. (2000);  $c_p$ , the specific heat of  
 462 air at constant pressure ( $J \text{ kg}^{-1} \text{ K}^{-1}$ );  $\gamma$ , the psychrometric constant ( $kPa \text{ K}^{-1}$ );  $\Delta$ , the  
 463 slope of the saturated vapor pressure curve ( $kPa \text{ K}^{-1}$ );  $D_m$ , vapor pressure deficit at  
 464 canopy source height ( $kPa$ ), assumed to be located at the apparent sink for momentum  
 465 ( $d+z_0$ , sensors were located at  $z=2$  m in our plots);  $\rho$ , air density ( $kg \text{ m}^{-3}$ ); and  $n = 2$  for  
 466 hypostomatous leaves (stomata present only on the lower surface of the leaf). The  
 467 resistance terms are:  $r_a$  ( $s \text{ m}^{-1}$ ), aerodynamic resistance above the canopy (between  
 468 source and reference heights), calculated according to Lhomme et al. (2012) for neutral  
 469 conditions as  $1/g_a$  (see Eq. 8);  $r_{a,f,h}$  ( $s \text{ m}^{-1}$ ), bulk boundary-layer resistance of the foliage

470 for sensible heat, calculated as  $r_{a,l} / 2LAI$ , with  $r_{a,l}$  the leaf boundary-layer resistance for  
 471 sensible heat and water vapor ( $s\ m^{-1}$ ), expressed as a function of the wind speed at  
 472 canopy height  $U(z_h)$  (Lhomme et al., 2012);  $r_{a,s}$  ( $s\ m^{-1}$ ), aerodynamic resistance between  
 473 the substrate (roughness length  $z_0=0.01\ m$ ) and the canopy source height ( $d+z_0$  different  
 474 in each plot, see 2.5) (Lhomme et al., 2012; Lhomme and Montes, 2014);  $r_{s,f}$  ( $s\ m^{-1}$ ),  
 475 bulk stomatal resistance of the foliage, isolated in Eq. 10 using  $E_t$  calculated with sap  
 476 flow data; and  $1/r_{s,f}$ , the estimated stomatal conductance of the foliage ( $G_s$ ).  
 477  $r_{s,s}$  is the substrate (soil and mulch) resistance to evaporation ( $s\ m^{-1}$ ), or the resistance to  
 478 water vapor movement from the interior to the surface of the soil. It is strongly  
 479 dependent on the water content of the upper soil surface layer. Soil layer surface  
 480 resistance  $r_s$  was calculated as (Anadranistakis et al., 2000):

$$481 \quad r_s = r_{s\ min} f(\theta_s) \quad (12)$$

$$482 \quad f(\theta_s) = 2.5 \left( \frac{\theta_{fc}}{\theta_s} \right) - 1.5 \quad (13)$$

483 where  $r_{s\ min}$  is the minimum soil surface resistance, which corresponds to soil moisture  
 484 at field capacity ( $\theta_{fc}$ ) and its value is assumed equal to  $100\ s\ m^{-1}$  (Thompson et al.,  
 485 1981, cit. in Zhang et al., 2008); and  $\theta_s$  is the water content of an upper soil surface  
 486 layer ( $cm^3\ cm^{-3}$ ), calculated by linear interpolation of our soil moisture readings (at 5, 15  
 487 and 30 cm) to 1 cm.

488 When an extraneous mulch is on top of a dry layer of soil  $r_{s,s} = r_s + r_m$ , with  $r_m$  transport  
 489 resistance of extraneous mulch ( $s\ m^{-1}$ ), resistance of mulch was calculated following  
 490 Fuchs and Hadas (2011):

$$491 \quad r_m = r_d - r_x \left[ 1 - \exp\left(-\frac{h_m}{h_x}\right) \right] \quad (14)$$

$$492 \quad r_d = \frac{h_m}{D_{eff}} \quad (15)$$

493 where  $r_d$  is the diffusive component of the vapor transport resistance defined as the ratio  
 494 of the thickness of the mulch ( $h_m$ , average 0.0461 m for both plots) over the effective  
 495 diffusivity of water vapor in the porous medium ( $D_{\text{eff}} = 1.05 \cdot 10^{-5} \text{ m}^2 \text{ s}^{-1}$  according to  
 496 Flurry et al., 2009).  $r_x$  and  $h_x$  are fitting parameters (Fuchs and Hadas, 2011) that depend  
 497 on the wind speed at 0.125 m (estimated according to Wang, 2014).  
 498 Finally, to obtain  $r_{s,s}$  for the area of the plots, resistances for the different surface covers  
 499 ( $r_s$  and  $r_m$ ) were weighted according to the proportion of bare soil (21.5 and 22.6% for C  
 500 and T, respectively), the proportion covered by mulch and litter (53.0 and 48.5% for C  
 501 and T) and the proportion of surface covered by rock fragments/outcrops (25.5 and  
 502 28.8% for C and T). The resistance of the latter was fixed to the highest value of  
 503 resistances found in our data set ( $21,500 \text{ s m}^{-1}$ ), assuming that its evaporation will be  
 504 close to zero.

505 In S-W's original study,  $\lambda ET = \lambda E_t + \lambda E_s$ , but here we followed the modified expression  
 506 from Lhomme et al. (2012):

$$507 \quad \lambda E = \left( \frac{\Delta + \gamma}{\gamma} \right) \frac{(R'_f + R'_s)r_a}{R'_f R'_s + R'_a (R'_f + R'_s)} \left( \frac{\Delta A + \rho C_p \frac{D_a}{r_a}}{\Delta + \gamma} \right) + \frac{\Delta}{\gamma} \left( \frac{R'_s A_f r_{a,f,h} + R'_f A_s r_{a,s}}{R'_f R'_s + R'_a (R'_f + R'_s)} \right) \quad (16)$$

508 where  $R'$  are the modified resistances terms (aerodynamic, foliage and substrate)  
 509 (Lhomme et al., 2012) from the original  $R$  terms in the S-W model:

$$510 \quad R'_f = \frac{R_f}{\gamma} = r_{s,f} + \left( n + \frac{\Delta}{\gamma} \right) r_{a,f,h} \quad (17)$$

$$511 \quad R'_s = \frac{R_s}{\gamma} = r_{s,s} + \left( 1 + \frac{\Delta}{\gamma} \right) r_{a,s} \quad (18)$$

$$512 \quad R'_a = \frac{R_a}{\gamma} = r_a + \left( 1 + \frac{\Delta}{\gamma} \right) \quad (19)$$

$$513 \quad R_f = (\Delta + n\gamma)r_{a,f,h} + \gamma r_{s,f} \quad (20)$$

$$514 \quad R_s = (\Delta + \gamma)r_{a,s} + \gamma r_{s,s} \quad (21)$$

$$515 \quad R_a = (\Delta + \gamma)r_a \quad (22)$$

516 The difference between  $E$  (ET) in Eq. 16 and the sum of  $E_t$  (sap flow data) and  $E_s$  (Eqs.  
517 10 and 11) was considered as a miscellaneous residual term ( $E_r$ ) including shrub  
518 evapotranspiration, damp litter evaporation and errors from calculations.

### 519 2.7. Data analysis

520 Differences between control and treated plots were analyzed with ANOVA (treatment  
521 and block as fixed factors) or, alternatively, a non-parametric Kruskal–Wallis test was  
522 used when data did not fulfill the assumption of homoscedasticity (this was the case for  
523 sap flow variables, sorted by diameter classes). We studied the relative contribution of  
524 the treatment, atmospheric variables and tree structure metrics on tree transpiration. To  
525 this end, relationships were investigated through Pearson correlations and multiple  
526 linear regression models. The regression models are not intended for predictive  
527 purposes but for quantifying the relative importance of the different independent  
528 variables (treatment, atmospheric variables and tree metrics) in explaining the variance  
529 of  $v_s$  and  $S_f$  (dependent variables). The relative importance of any independent variable  
530 was computed from its individual contribution to the sum of squares in the regression  
531 model. We performed stepwise multiple linear regression (MLR) for fitting the  
532 regression models in order to account only for independent variables that explained  
533 additional variance (criterion to select a variable:  $F$  probability for including  $< 0.05$ ;  $F$   
534 probability for excluding  $> 0.10$ ). The residuals were examined for normality,  
535 independence and homoscedasticity (Q-Q plots), linearity between dependent and  
536 independent variables was assessed (Pearson coefficient) and autocorrelation and  
537 multicollinearity in independent variables were checked through the Durbin-Watson  
538 coefficient and tolerance, respectively. Statistical proofs took into account only  
539 measured data, i.e. data calculated to fill in gaps were excluded and were used only for  
540 year-round balances. The cumulative effect of the treatment on  $E_t$  and  $E_s$  was evaluated

541 in terms of a shift in the daily ratio of treated/control following the intervention: In  
542 (T/C) (Perry and Jones, 2016). Because of the complete block design layout, we  
543 assumed baseline (in the pre-operational period) to be zero. A significance level of  
544  $p < 0.05$  was used for all analyses. Data were handled and analyzed with Excel, SPSS  
545 20.0 and R studio software (RStudio Team, 2015).

### 546 **3. Results**

#### 547 *3.1 Meteorological data*

548 Annual precipitation during the study period was usually below the area average of 466  
549 mm, with 405 mm (2013), 354 mm (2014), 320 mm (2015) and 499 mm (2016), i.e.  
550 only the most recent year was wetter than the average (Figure 1). However, by water  
551 years, the figures changed notably, with 534, 271, 426 and 297 mm for water years  
552 2012-2013 to 2015-2016, respectively, where 2014 came out as very dry (Pg between  
553 Jan 1<sup>st</sup> to Sep 20<sup>th</sup> accumulated only 139 mm) and 2013 as very wet, with marked  
554 influence on the soil moisture pattern (Figure 1). Temporal trends of temperature were  
555 closely coupled with seasonal variation: the coldest period was recorded between late  
556 January and early February 2015 (daily average  $-2.3^{\circ}\text{C}$ , minimum  $-10.4^{\circ}\text{C}$ ), and the  
557 hottest days occurred in the summer of the same year (daily average and daily  
558 maximum T were above 26 and  $37^{\circ}\text{C}$ , respectively, for most of the days between late  
559 June and early August that year). Mean value of T in 2013,  $11.1^{\circ}\text{C}$ , contrasts with those  
560 of the following years: 12.2, 12.0 and  $12.5^{\circ}\text{C}$  in 2014, 2015 and 2016. Temporal trends  
561 of D and  $R_{s,a}$  were also coupled with seasonal variation (Figure 1), with high inter-  
562 annual variability too: mean D in 2013 (0.52 kPa) contrasts with that of the following  
563 years (0.59, 0.63 and 0.59 kPa for 2014 to 2016).

#### 564 *3.2 Tree growth traits and stand structure*

565 Growth traits were affected after the clearing treatment in different ways. Shoot length  
566 and diameter were not affected by the treatment, whereas the number of leaves, leaf area  
567 and SLA were all significantly affected (Table 2). In the crown, the number of shoots  
568 per branch increased significantly in the cleared plot from 35 to about 49 shoots, and the  
569 tree-based LAI was also higher there (0.93 and 0.81 m<sup>2</sup> m<sup>-2</sup> for T and C, respectively),  
570 though not significantly. In addition, sorting the data by diameter class and year  
571 changed several of these results (Figure 2). The presence of epicormic shoots and stump  
572 sprouts in T that came out in 2014, but became much more apparent in 2015, is also  
573 worth mentioning. These shoots generally had two growth cycles (spring and autumn)  
574 and morphological features that were far above the values of the shoots in the crown  
575 (Table 2).

576 Ground-based LAI followed a seasonal variation pattern in both plots, with the lowest  
577 values reached in summer, matching the period of foliage throughfall (Figure 3). Except  
578 for the re-sprouts and epicormic shoots, the leaf carriage period was found to spread  
579 from spring to summer of the following year (about 15 months) in both plots. That  
580 made summer LAI fluctuate sharply, dropping to 0.58 and 0.35 m<sup>2</sup> m<sup>-2</sup> for C and T,  
581 respectively, in the driest period in summer 2014. LAI was higher in C than in T until  
582 spring 2016, when a decreasing trend in C made the series of the thinned plot catch up  
583 with that of the untreated trees. In fact, by the end of the study, summer LAI in T  
584 reached values close to those measured before thinning in May 2012.

### 585 *3.3 Sap flow, tree-water use and soil moisture*

586 Sapwood depth varied between 3.18 and 7.55 cm into the xylem, which accounted for  
587 between 62 and 100% of the BA of the sampled trees. Sapwood area (Sa) was strongly  
588 related either to D<sub>BH</sub> or to tree BA (Sa=1.453D<sub>BH</sub><sup>1.6794</sup>, r = 0.964; Sa=0.652BA+17.425,

589  $r = 0.982$ , units either in cm or  $\text{cm}^2$ ). In C and T plots, mean Sa values in the sampled  
590 trees were  $139 \pm 110$  and  $218 \pm 228 \text{ cm}^2$ , respectively.

591 Both mean sap flow velocity ( $v_s$ ) and mean sap flow ( $S_f$ ) per tree had a wide range of  
592 values throughout the study period (Figure 4). Even so, the effect of the treatment was  
593 highly significant ( $p \leq 0.001$ ) in all diameter classes (DC). In the control,  $v_s$  and  $S_f$   
594 averages, either for the entire period or the growing season period (Mar-Oct), were just  
595 48 and 35% respectively of the treatment averages in the lower DC, or 66 and 40% (for  
596  $v_s$  and  $S_f$  respectively) in the dominant/co-dominant DC's. Thus, the effect of thinning  
597 on tree transpiration was proportionally higher in the smaller trees. On average, a  
598 dominant or co-dominant tree in the treatment consumed  $22.4 \text{ l day}^{-1}$  during the  
599 growing season (or  $18.5 \text{ l day}^{-1}$  when averaging over the entire period), whereas a tree  
600 in the control took up only  $9.0 \text{ l day}^{-1}$  (or  $7.5 \text{ l day}^{-1}$  in the entire period). However,  
601 these values are biased by the different means in tree Sa between treatments; on  
602 normalizing by this metric, the above values correspond to  $0.089 \text{ l day}^{-1} \text{ cm}^{-2}$  and  $0.047 \text{ l}$   
603  $\text{day}^{-1} \text{ cm}^{-2}$  for T and C in the growing season, or  $0.073 \text{ l day}^{-1} \text{ cm}^{-2}$  and  $0.039 \text{ l day}^{-1} \text{ cm}^{-2}$   
604 for T and C in the whole period.  $v_s$  showed higher values in T trees in the lower DC1-2  
605 than in C trees in the higher DC3-4 (Figure 4).

606 As well as thinning treatment and tree size, other variables relating to atmospheric  
607 conditions, soil moisture and date were also linearly related to the transpiration  
608 variables  $v_s$  and  $S_f$  at different temporal scales (Table 3). Among them, the linear  
609 correlations with date, T,  $R_{s,a}$  and D stand out, although they are from moderate to low  
610 ( $r < 0.5$ ) depending on both the period under consideration (growing season vs. entire  
611 period) and the time scale. The significant correlations in the date-related variables  
612 indicate that, in the span of our study, transpiration showed an increasing trend, in  
613 parallel with the observed trend in D and T. Soil moisture ( $\theta$ ) and transpiration showed

614 opposite temporal patterns (negative relationship) that persisted regardless of the  
615 temporal scale when looking at the entire period, although that correlation weakened or  
616 even became insignificant when considering only the growing season. Figure 1 shows  
617 that  $\theta$  had a general seasonal trend responding to  $P_g$ , but with slight differences between  
618 T and C throughout the temporal span 2012-2016. During the first year (2012),  $\theta$  was  
619 higher in T (47% and 56% of  $\theta_{rel}$  at 15 cm for C and T, respectively), and this difference  
620 increased with the depth of the soil (absolute  $\theta$  at 5, 15 and 30 cm was 15.1, 18.4 and  
621 21.2% respectively for C and 16.3, 21.9 and 25.6% for T). On the contrary, during the  
622 rainy year 2013, the differences were absent ( $\theta_{rel}$  46% and 44% on average in C and T,  
623 respectively), but appeared again in the following dry year 2014 ( $\theta_{rel}$  28% and 39% for  
624 C and T). In the final two years, both plots showed similar values again (about 36%  
625  $\theta_{rel}$ ).

626 The MLR models fitted to study the relative importance of the independent variables in  
627 the explained variance of transpiration (filtered by growing season and daylight hours)  
628 were significant in all cases, although some of them showed autocorrelation and  
629 multicollinearity, together with limited explanation of variation (Table 4). However,  
630 beyond their predictive ability, they showed that the treatment and the structure of the  
631 tree (which is also directly affected by the treatment) were the most important variables  
632 in explaining both  $v_s$  and  $S_f$  at the different temporal scales considered. The treatment  
633 accounted for about a quarter of daily transpiration; and the size of the trees, for an  
634 additional half. As the treatment affects the frequency distribution of the diameter  
635 classes, it can be assumed that the size of the mean tree in the thinned plot is affected by  
636 the treatment. Weighted by  $r^2$ , the treatment explained about 20% of total variance in  
637 daily  $S_f$ .

638 *3.4. Response of  $G_s$  to environmental ( $\theta$  and  $D$ ) constraints*

639  $G_s$  was studied to better address the effect of the treatment on how  $\theta$  and D constrained  
640 carbon and water fluxes. The relationship between  $G_s$  and D showed a clear logarithmic  
641 response, which was markedly affected by limitation from  $\theta$  (Figures 5, 6), with low  $G_s$   
642 and  $G_{sref}$  and low sensitivity to D ( $-m$ ) when the soil was dry ( $\theta_{rel}<0.2$ ) regardless of the  
643 treatment. In spite of the similar sensitivity to D in both treatments under dry soil,  $G_s$   
644 and  $G_{sref}$  remained higher in the T plot. However, under wetter soil conditions ( $\theta_{rel}>0.4$ ),  
645 both  $G_s$  and  $G_{sref}$  were higher and more responsive to D (Figures 5, 6), showing higher  
646 stomatal sensitivity, especially in the control plot ( $-m$  was 0.71 and 0.43 in C and T,  
647 respectively). Above severe soil water deficit ( $\theta_{rel}>0.2$ ),  $G_{sref}$  remained constant in T but  
648 still increased in C between  $0.2<\theta_{rel}<0.4$  and  $\theta_{rel}>0.4$ , indicating more  $\theta$  limitations on  
649  $G_s$  in the latter. Likewise, lower values absolute values of  $m$  in T indicated less stomatal  
650 responsiveness to increasing D, and hence the carbon and water fluxes were less  
651 affected by air dryness. The slope of  $-m$  to  $G_{sref}$  was found to be in most cases less than  
652 0.6: between 0.30 and 0.65 in C and between 0.22 and 0.50 in T (Figure 6a).

### 653 *3.5. Stand transpiration ( $E_t$ ) and dry canopy evapotranspiration partitioning*

654 For the distribution of diameters in both plots as well as tree density (Table 1), the  
655 previous  $S_f$  values corresponded to  $0.253\pm 0.153$  and  $0.248\pm 0.162$  mm transpired per  
656 day in the entire period for C and T, respectively, and  $0.317\pm 0.152$  and  $0.306\pm 0.156$   
657 mm transpired per day in C and T in the growing season (Mar-Oct) (Figure 7). These  
658 values of  $E_t$  were variable between years, with 2013 having the lowest daily mean in  
659 both plots ( $0.211\pm 0.117$  and  $0.159\pm 0.096$  mm day<sup>-1</sup> for C and T, respectively) and the  
660 years 2014 and 2015 showing the highest daily means for C ( $0.297\pm 0.183$  mm day<sup>-1</sup> in  
661 2014) and T ( $0.332\pm 0.178$  mm day<sup>-1</sup> in 2015) (Figure 7). Non-parametric tests indicated  
662 no significant differences between C and T in  $E_t$ . Annually, the canopy of holm oaks in

663 C transpired between 77 mm in 2013 and 108 mm in 2014 (Table 5), whereas in T these  
664 values ranged between 58 mm (2013) and 121 mm (2015) (Table 5).

665 The physically-based model of S-W allowed a further partitioning of total dry canopy  
666 ET into its different components (Table 5 and Figures 7, 8). The greater contribution of  
667 soil evaporation ( $E_s$ ) to total ET in the treated plot (~40% of ET) than in the control plot  
668 (~28% of ET) stands out. On a daily basis, T always showed higher  $E_s$  than C did  
669 ( $0.212 \pm 0.216$  and  $0.124 \pm 0.123$  mm day<sup>-1</sup> for T and C, respectively), with significant  
670 differences ( $p < 0.001$ ). Also, inter-annual variability in  $E_s$  was lower than in  $E_t$  (or  $E_r$ ),  
671 with mean annual values (2013-2016) ranging between 0.122 and 0.139 mm day<sup>-1</sup> in the  
672 control and 0.180-0.245 mm day<sup>-1</sup> in the treatment. The residual term,  $E_r$ , including the  
673 unaccounted understory transpiration, litter evaporation and noise, was slightly higher  
674 in C ( $0.067 \pm 0.109$  mm day<sup>-1</sup>, 15% of ET) than in T ( $0.063 \pm 0.105$  mm day<sup>-1</sup>, 12% of ET)  
675 and ranged between 0.033 and 0.041 mm day<sup>-1</sup> for C (2014) and T (2013), respectively,  
676 and between 0.127 and 0.120 mm day<sup>-1</sup> for C and T in 2015.

677 The components of ET showed a typical seasonal pattern in both plots, with most of the  
678 evaporation occurring during summer and spring. It is clear that, in the span of this  
679 study,  $E_t$  in the treatment (T) surpassed that of the control (C) during the main dry  
680 spells, from mid-July onwards (Figure 8 and Figure 9,  $\ln [E_{t\_T}/E_{t\_C}]$ ), indicating that  
681 the cleared oaks are using a water reservoir that is not available to the control trees  
682 during summer months. In fact, annual balances (Table 5) show that the difference C  
683 minus T for annual  $E_t$  ranged from +19 mm (2013) to -16 mm (2015).

#### 684 4. Discussion

685 The results showed that the silvicultural treatment affected the variables studied at  
686 different spatial (tree and stand) and temporal scales.

##### 687 4.1 Growth and leaf traits

688 The forest treatment enhanced growth as compared to the control plot, as expected.  
689 Increased height and diameter growth in holm oak after thinning have been previously  
690 reported under similar conditions (Mayor and Rodà, 1993; López et al., 2003; Cotillas et  
691 al., 2009; Gea-Izquierdo et al., 2009; Cabon et al., 2018). Annual shoot growth results  
692 from equilibrium between endogenous growth processes and exogenous constraints  
693 exerted by the environment (Barthélémy and Caraglio, 2007), which were  
694 experimentally altered in our study. However, the length of the growing season's shoots  
695 (a surrogate for height growth) was only marginally affected (only in 2013). Rather, it  
696 was the leaf traits (leaves per shoot and number of shoots per dominant branch in a tree)  
697 that were most enhanced by the treatment, which corroborates similar results previously  
698 reported in the species (López et al., 2003). The treated trees had higher SLA and lower  
699 leaf mass area ( $LMA=1/SLA$ ) than the trees in C. LMA is a key trait that reflects the dry-  
700 mass cost of making new leaf area, whilst leaf lifespan represents the duration over  
701 which photosynthetic revenue is returned (Wright et al., 2004). As we found no  
702 difference in lifespans between C and T (about 15 months), the cost of deploying new  
703 leaves was higher in C, which meant that its resource-use strategy was more  
704 conservative (Stahl et al., 2014). In evergreen shrubs and trees growing in harsh climate,  
705 high LMA correlates negatively with rainfall (Wright et al., 2004), and net rainfall was  
706 indeed lower in the control plot (del Campo et al., 2018). Our tree-based LAI was also  
707 higher in the treatment, although not significantly, reinforcing the idea that leaf traits were  
708 particularly affected by the treatment. Growth was very variable inter-annually, with some  
709 years (2013 and 2015) showing less growth than others (2014 and 2016), which is  
710 especially true for the trees in the control (Figure 2). 2013 was the coolest and rainiest  
711 year, with a mean T of 8.4°C in the Jan-Jun period, 1.6°C lower than the corresponding T  
712 of the following year. This probably had an impact on most growth traits in both C and T,

713 which had minima that year. However, it had a positive impact on the following year's  
714 growth in both plots, even though 2014 was the driest year: available resources were first  
715 used to build new shoots and leaves. This meant that growth was positively enhanced by  
716 the previous year's precipitation, as reported earlier for holm oak (Gea-Izquierdo et al.,  
717 2009) and for pine trees at a nearby site (Fernandes et al., 2016). 2015, following the  
718 previous year's pronounced drought, with moderate  $P_g$  in late spring-early summer and  
719 high summer temperatures, had a negative impact on growth in C trees, but almost no  
720 effect on the dominant-codominant trees of T. The combined effects of the treatment and  
721 climate-growth relationships can be better observed in  $E_t$  in 2015 (Table 5): with total ET  
722 increasing,  $E_t$  decreased in C, whilst T showed the highest tree-water use and  $E_t$  values of  
723 the series. The impact of thinning on growth also depended on the size of the trees (Figure  
724 2), so that growth was higher in larger trees than in smaller ones, as previously reported  
725 (Mayor and Rodà, 1993). *Quercus ilex* may show several growth units annually or  
726 polycyclism (Barthélémy and Caraglio, 2007; Barbeta and Peñuelas, 2016), which is  
727 related to the meteorological conditions in the current and previous years (Girard et al.,  
728 2011). In our plots, we only observed one annual shoot growth unit (monocyclism) on  
729 the trees in either C or T, with the exception of re-sprouts and epicormic shoots, which  
730 had two cycles. The importance of the re-sprouting growth from 2015 onwards cannot be  
731 overlooked, as both epicormic shoots (in pruned trees) and stump sprouts were notably  
732 enhanced with the treatment. This undesirable feature is typical of the species, as it is  
733 likely to cause rapid decline in the positive effects of clearing in the first three years after  
734 the treatment (Cotillas et al., 2009). In our case, vigorous re-sprouting shoots, although  
735 shorter than in Cotillas et al.'s study (~ 25 cm in the reference vs. 13 cm in this study), are  
736 probably related to the relative increase of the  $E_r$  term in the treatment in 2015.

#### 737 4.2 Tree and stand-water use

738 Transpiration notably increased with thinning both on a tree basis and at stand scale,  
739 especially during the summer months of the second half of the study period. Daily tree-  
740 water use in the dominant and co-dominant trees in T ( $22.4 \text{ l tree}^{-1}$  in the growing  
741 season) was very close to the values reported in Reyes-Acosta and Lubczynski (2013)  
742 for the same species at low density and with similar-sized trees ( $D_{\text{BH}}$ : 22-31 cm,  $\sim 21 \text{ l}$   
743  $\text{tree}^{-1}$ ). These authors also reported stand transpiration between  $0.26\text{-}0.48 \text{ mm day}^{-1}$  for  
744 areas with tree densities between  $181\text{-}280 \text{ trees ha}^{-1}$ , which again confirms our growing  
745 season transpiration in the treated trees ( $0.31 \text{ mm day}^{-1}$  for a density of  $299 \text{ trees ha}^{-1}$ ).  
746 However, other studies with sparse stand (Infante et al., 2003) have reported both higher  
747 tree-water use (between  $24 \text{ l tree}^{-1} \text{ day}^{-1}$  -autumn/winter- and  $80 \text{ l tree}^{-1} \text{ day}^{-1}$  -  
748 spring/summer) in trees of a similar size to our dominant oaks in the thinned plot, and  
749 higher stand transpiration ( $169\text{-}205 \text{ mm year}^{-1}$ ). In spite of the similarity in canopy  
750 cover between that study (34%) and our treatment plot, the higher LAI ( $1.9 \text{ m}^2 \text{ m}^{-2}$ ) at  
751 that site may explain the differences. Moreno and Cubera (2008) provided an empirical  
752 fit between stand  $E_t$  and cover in a warmer site on deep soil that, when used with our  
753 data, gives stand  $E_t$  between  $0.55\text{-}0.86$  and  $0.43\text{-}0.57 \text{ mm day}^{-1}$  for C and T,  
754 respectively. Our plots, especially the control, remain out of that range. Other studies  
755 dealing with holm oak transpiration in wetter climates and higher LAI (Limousin et al.,  
756 2009) also reported higher values of stand  $E_t$  ( $243\text{-}430 \text{ mm year}^{-1}$   $P_g > 680 \text{ mm}$ ; LAI:  
757  $1.5\text{-}1.9 \text{ m}^2 \text{ m}^{-2}$ ). Thus, sap flow values in this study are the lowest among those found in  
758 the literature, which confirms the marginality of this population and the appropriateness  
759 of adaptive management. The values reported in a nearby experiment in thinned Aleppo  
760 pine were lower ( $5.2$  and  $17.8 \text{ l tree}^{-1} \text{ day}^{-1}$  for similar covers to C and T, respectively)  
761 (del Campo et al., 2014), which might be due to the different water use strategies of the  
762 two species (Martínez-Ferri et al., 2000).

763 Apart from the treatment and the size of the trees, tree transpiration was mostly  
764 explained by variation in  $D$  and other atmospheric driving variables, with no or negative  
765 influence of  $\theta$  (negative relationship in short time scales and no relation at the growing  
766 season scale). The increase of transpiration with time along the span considered in this  
767 study coincides with an observed parallel increase in  $D$  (Figure S1. Supplementary  
768 Material). Other studies (Infante et al., 2003; Reyes-Acosta and Lubczynski, 2013) also  
769 reported no effect of  $\theta$  or drought on the transpiration of holm oaks, arguing either  
770 strong stomatal regulation or the access of tapping roots to the water-table that satisfied  
771 the need of water whenever demanded, which is a well-known response in this species  
772 (Barbeta and Peñuelas, 2016). Large trees have large root diameters that exert greater  
773 force and have greater ability to penetrate shallow and stony soils (López et al., 1998).  
774 This adaptation to stoniness makes large trees very resilient as they are able to prevent  
775 water stress and maintain a favorable leaf water balance by tapping water from deep soil  
776 layers. As  $\theta$  was affected after clearing, especially in the first 2-3 years of the study,  
777 deep water reservoirs must be affected too (in the wet year 2013, there was evidence of  
778 deep water recharge in both plots); during the driest year 2014, the differences were  
779 especially important. However, this variable had a transient effect, and by 2015 the  
780 differences between both plots had almost disappeared. This is consistent with previous  
781 results reported by Cotillas et al. (2009), who found significant differences in soil  
782 moisture associated with thinning only in the first year after the treatment.

783 The unexpected finding in our study is that  $E_t$  in the T plot slightly decreased with  
784 respect to C during the first half of the studied span, and caught up with it in the second  
785 half, with no significant differences over the whole period. The decrease in stand  $E_t$   
786 following a reduction in density and/or cover is a common response that has been  
787 widely reported (Moreno and Cubera, 2008; Limousin et al., 2009; Ungar et al., 2013;

788 del Campo et al., 2014; Ilstedt et al., 2016). The explanation for this is grounded in the  
789 very different frequency of age classes after the treatment, together with the very low  
790 water consumption observed in the lower DC in the control ( $0.062 \text{ l tree}^{-1} \text{ h}^{-1}$ ). This  
791 implied  $49 \text{ l h}^{-1}$  for a total of  $808 \text{ trees ha}^{-1}$ , whereas in the treatment that amount  
792 decreased by only one half ( $24 \text{ l h}^{-1}$ ) for about 18% of the trees (total of  $134 \text{ trees ha}^{-1}$  in  
793 DC1-2). In the higher DC's, these figures rose to 102 and  $141 \text{ l h}^{-1}$  in C and T,  
794 respectively, for a total of 325 and  $183 \text{ trees ha}^{-1}$ . The number of trees in the highest DC  
795 remained essentially the same in the treatment (127 and  $109 \text{ trees ha}^{-1}$  in C and T,  
796 respectively), while its water use was more than twice that of the control. Smaller tree  
797 size and heavy competition might worsen the effect of extreme droughts on tree vigor  
798 (Barbeta and Peñuelas, 2016; Gentilesca et al., 2017). Moreover, the reported lag of the  
799 response to thinning for fine root growth is about 1.5 years (López et al., 2003), a span  
800 that in our case would explain why during the first months/year after clearing  $E_t$  was  
801 slightly higher in C, whilst in the second half of our study period T figures began to  
802 depart from C in this water flux. The increase in fine root biomass after thinning has  
803 been reported for similar conditions (López et al., 2003) and is probably the response to  
804 higher net precipitation, soil temperature and soil nutrient content. The slash from  
805 thinning was left on the soil and had a significant effect on the mineralization of organic  
806 matter and a subsequent fertilization effect (unpublished data).

#### 807 *4.3 Environmental controls on $G_s$*

808 Low water availability in the soil ( $\theta_{\text{rel}} < 0.2$ ) reduced  $G_{s\text{ref}}$  and stomata responsiveness to  
809 D (-m) in both plots, with the advantage of smaller absolute change in  $G_s$  with  
810 increasing D. Under water stress, *Q. ilex* shows great stomatal control to avoid low leaf  
811 water potentials and minimize the risk of xylem cavitation (Martinez-Vilalta et al.,  
812 2003; Barbeta and Peñuelas, 2016). Therefore,  $G_s$  remained at low values regardless of

813 D. However, the treated oaks showed slightly higher  $G_{sref}$  and hence less  $\theta$  limitation on  
814  $G_s$ , which was supported by the high tree-water use observed in this plot during the dry  
815 spells (Figure 9). This implied that, in spite of the dry conditions that prevailed during  
816 most of our study span, these trees maintained water and carbon dynamics at higher  
817 rates than the control. This higher  $G_{sref}$  under  $\theta$  limitation can be considered as an active  
818 acclimation in the thinned trees, which may be due to the development of deeper roots  
819 (Grossiord et al., 2017). With plenty of soil moisture ( $\theta_{rel}>0.4$ ),  $G_{sref}$  and  $-m$  increased  
820 markedly, especially in the C trees, in which the greater sensitivity of  $G_s$  to D is  
821 indicative of higher stomata responsiveness to air dryness, i.e. they are more reactive to  
822 stimuli that may provoke their closure. Higher sensitivity ( $-m$ ) has the disadvantage of  
823 having greater absolute reduction in  $G_s$  with increasing D in spite of soil water  
824 availability. This might be due to quicker water depletion in the overstocked control  
825 plot and the subsequent risk of loss of hydraulic conductivity at high D (Oren et al.,  
826 1999). Hydraulic conductivity is a key trait to be maintained in holm oak trees, as  
827 embolism recovery is much more limited than in other co-occurring species (Trifilò et  
828 al., 2015). It is also important to highlight the different response in  $G_{sref}$  between classes  
829  $0.2<\theta_{rel}<0.4$  and  $\theta_{rel}>0.4$  in both treatments: in T,  $G_{sref}$  remained essentially constant  
830 between the two classes, thus reflecting no  $\theta$  limitation and stomatal acclimation (size,  
831 density and/or osmotic adjustment) so that trees are less responsive to air dryness  
832 (Grossiord et al., 2017). On the other hand,  $G_{sref}$  increased in C, indicating that  $\theta$   
833 limitations still persisted in the class  $0.2<\theta_{rel}<0.4$  (absolute  $\theta$  between 10 and 16%), as  
834 compared to class  $\theta_{rel}>0.4$  (absolute  $\theta>16\%$ ).

835 Whenever the stomata are regulating leaf water potential near a constant value, a slope  
836 close to 0.6 is expected (Oren et al., 1999). In our case, the wider range of D in the  
837  $\theta_{rel}<0.4$  classes and the very low influence of boundary layer conductance (mean values

838 of the decoupling coefficient  $\Omega$  were below 0.1, indicating high coupling to D, Figure  
839 S2. Supplementary Material) may explain why in most cases our data are below the 0.6  
840 slope (Oren et al., 1999).

#### 841 *4.4 ET partitioning*

842 The significant increase in soil evaporation ( $E_s$ ) after clearing was the main impact of  
843 the treatment on ET partitioning. The value of  $E_s$  calculated in our plots was in the  
844 range of values previously reported in the literature and validate the S-W approach of  
845 this study. For instance, in a similar climate with the same species, Balugani et al.  
846 (2011) reported daily bare soil evaporation in the dry season of  $0.55 \text{ mm day}^{-1}$ , with  
847  $0.28 \text{ mm day}^{-1}$  of this corresponding to the unsaturated zone evaporation and the  
848 remainder to the saturated water zone. In our plots, spots of saturated water are assumed  
849 to exist locally in deep fractured rock; during the March-October period the daily mean  
850 was  $0.17$  and  $0.29 \text{ mm day}^{-1}$  for C and T, respectively. Other studies on the  
851 Mediterranean (Raz-Yaseef et al., 2010a) have reported higher ranges of  $E_s$  ( $0.24$  to  $3.6$   
852  $\text{mm day}^{-1}$ ) and higher  $E_s/P_g$  ratio (30-53%) at a warmer and drier site. The important  
853 result in our study is that this component made total ET higher in the treated plot on  
854 average, as  $E_t$  did not differ substantially between treatments. However, closer  
855 examination of the temporal trends (Figure 9 bottom) reveals that, during wet spells, ET  
856 remained lower in the treated plot whereas in dry spells the pattern was reversed. In this  
857 regard, it appears that the dominance of dry years during our study period biased the  
858 overall average. Also, in the treated plot, the contribution of  $E_s$  to total ET decreased  
859 from about 50% in 2013 to around 35% in the following years, close to the range  
860 reported for the Yatir forest (36-38%) in Israel (Raz-Yaseef et al., 2010b). Wet canopy  
861 evaporation (interception,  $E_i$ ) is not shown here, although it was monitored  
862 simultaneously (del Campo et al., 2018). Figure 9 (up) shows total accumulated dry and

863 wet canopy evaporation ( $ET+E_i$ ) and similar conclusions: in the drier spells in 2014 and  
864 2015 the control plot used slightly less water than the treatment, whereas in the first  
865 wetter half of the study period, the control plot used significantly more water. The main  
866 point is that the ET differences between treatment and control took place in dry spells,  
867 from mid-summer to early autumn, so that the increased net precipitation in the T plot  
868 was used later on for  $E_t$ , mainly in the bigger oaks.  $G_s$  was in fact higher in the dry  
869 spells in T, as already mentioned. In addition to the wet and dry spells' turnover, Figure  
870 9 also confirms the lagged effect after thinning of about 1.5 years, supporting that root  
871 growth might have enhanced the stand  $E_t$  (López et al., 1998, 2003). Also, stump  
872 regrowth was marked after 2014. This means that  $E_s$  and  $E_t$  tend to offset mutually, as  
873 seen in the final year (Table 5). These results contrast with previous values obtained  
874 nearby in a 70 year-old Aleppo pine plantation (del Campo et al., 2014). Apart from the  
875 important difference in Pg in that study (1,545 mm in 25 months), these authors found  
876 no greater increase in stand  $E_t$  or ET in the thinned trees than in the control, which could  
877 be because, during rainy periods without soil moisture restriction, the control is able to  
878 take up much more water because of the number of trees. However, in drier years, soil  
879 water limits  $G_s$  in the control and fewer well-watered trees in the treatment can surpass  
880 the  $E_t$  of the control. The finding that the main differences between the two treatments  
881 occurred during the dry spells supports this assertion. In this context, the difference Pg  
882 minus total ET in C ranged between 44 mm (2015) and 285 mm (2016) and between 19  
883 and 281 mm for T in the same years. The net mean difference between both plots across  
884 the years is of 65 mm of extra blue water (runoff and deep percolation; 15 mm per year)  
885 in T. Thus, the overall results given here show that the treatment mostly had a watering  
886 effect on a thirsty declining forest (Grant et al., 2013).

## 887 **5. Conclusions**

888 Key functional responses related to drought were triggered by thinning in a marginal  
889 forest that enhanced growth, carbon and water cycles. This performance was driven by  
890 leaf and growth traits that promoted a more efficient (and less conservative) use of  
891 resources, by improved stomatal behavior with regard to air dryness and declining soil  
892 moisture, and by increased deep-water access. The development of deep roots that  
893 enable access to deep-water reservoirs during dry spells is one of the key traits in the  
894 drought resistance of holm oaks (Barbeta and Peñuelas, 2016) and of other semi-arid  
895 species (Grossiord et al., 2017). From a water-balance point of view, the overall results  
896 reveal an increase in ET with the treatment, especially in  $E_s$ . Thinning from below  
897 resulted in little change in the frequency of oaks in the upper diameter classes (with  
898 significant water-use), which, together with decreased competition and increased net  
899 rainfall, fueled tree and stand-water use in the treatment, especially during the frequent  
900 dry spells recorded in our study. By the end of the study period,  $E_s$  and  $E_t$  in the  
901 treatment appeared to offset each other mutually due to higher soil coverage from  
902 stumps' regrowth. Thus, the net result in the 4-year span is a significant increase in ET  
903 and very limited decrease in total ET when adding wet canopy evaporation ( $E_i$ ).  
904 Additional monitoring is needed in order to assess the observed trends of both climate  
905 and vegetation. Data presented here demonstrate that this oak stand is experiencing a  
906 clear decline that has been counterbalanced by the effectiveness of forest management,  
907 with a profound effect on the carbon and water fluxes at tree and stand scales. This  
908 study may provide some generalizations or guidelines for eco-hydrology-oriented  
909 silviculture in stands experiencing tree encroachment and transformation into  
910 shrublands, that are more prone to global change-induced disturbances (droughts,  
911 blue/green water impairment, fire hazard, etc.). In this regard, rather than just defining a  
912 particular forest structure, silviculture must be thought to improve responses in i) key

913 growth and leaf traits such as SLA or LAI, with particular attention to its temporal  
914 dynamics; ii)  $G_s$  and its behavior with regard to declining soil moisture and increasing  
915 air dryness; and iii) tree-water use and deep water access. Also, under below-average  
916 rainfall conditions like those recorded here, improvement in blue water flows (run-off  
917 and groundwater) seems unlikely and such a potential side-effect cannot be used to  
918 argue in favor of adaptive management. Fewer trees led to higher  $\theta$ , but also to higher  
919  $E_s$ , with little change in the stand  $E_t$ . Thus, simplifying, we could say that the observed  
920 responses are not because of more water but because of fewer trees using a similar  
921 amount of water to that in the untreated stand.

## 922 **Acknowledgements**

923 This study is a component of the research projects HYDRASIL (CGL2011-28776-C02-  
924 02), SILWAMED (CGL2014-58127-C3-2) and CEHYRFO-MED (CGL2017-86839-  
925 C3-2-R), funded by the Spanish Ministry of Science and Innovation and FEDER funds.  
926 The authors are grateful to the Valencia Regional Government (CMAAUV, Generalitat  
927 Valenciana) and ACCIONA for their support in allowing the use of the experimental  
928 forest La Hunde and for their assistance in the fieldwork.

## 929 **References**

930 Allen, C.D., Macalady, A.K., Chenchouni, H., Bachelet, D., McDowell, N., Vennetier,  
931 M., Kitzberger, T., Rigling, A., Breshears, D.D., Hogg, E.H., Gonzalez, P., Fensham,  
932 R., Zhang, Z., Castro, J., Demidova, N., Lim, J.H., Allard, G., Running, S. W., Semerci,  
933 A., Cobb, N., 2010. A global overview of drought and heat-induced tree mortality  
934 reveals emerging climate change risks for forests. *For. Ecol. Manag.* 259, 660– 684.

935 Anadranistakis, M., Liakatas, A., Kerkides, P., Rizos, S., Gavanosis, J., Poulouvassilis,  
936 A., 2000. Crop water requirements model tested for crops grown in Greece. *Agric.*  
937 *Water Manage.* 45, 297–316.

938 Barbeta, A., Peñuelas, J., 2016. Sequence of plant responses to droughts of different  
939 timescales: lessons from holm oak (*Quercus ilex*) forests. *Plant Ecol. Diver.* 9(4), 321-  
940 338.

941 Balugani, E., Reyes-Acosta, J.L., van der Tol, C., Francs, A.P., Lubczynski, M.W.,  
942 2011. Partitioning and sourcing of dry season evapotranspiration fluxes at the foot-print  
943 of the eddy covariance tower in Sardón semi-arid location in Spain. *Estudios en la Zona*  
944 *no Saturada del Suelo*, X: 297-302.

945 Barthélémy, D., Caraglio, Y., 2007. Plant architecture: a dynamic, multilevel and  
946 comprehensive approach to plant form, structure and ontogeny. *Ann. Bot.* 99(3), 375-  
947 407. <http://doi.org/10.1093/aob/mcl260>

948 Bastiaanssen, W.G.M., Menenti, M., Feddes, R.A., Holtslag, A.A.M, 1998. A remote  
949 sensing surface energy balance algorithm for land (SEBAL): 1. Formulation. *J. Hydrol.*  
950 212-213, 198-212.

951 Berdanier, A.B., Miniati, C.F., Clark, J.S., 2016. Predictive models for radial sap flux  
952 variation in coniferous, diffuse-porous and ring-porous temperate trees. *Tree Physiol.*  
953 36(8): 929-931, doi:10.1093/treephys/tpw027

954 Bréda, N., Granier, A., Aussenac, G., 1995. Effects of thinning on soil and tree water  
955 relations, transpiration and growth in an oak forest (*Quercus petraea* (Matt.) Liebl.).  
956 *Tree Physiol.* 15 (5), 295-306.

957 Burgess, S.S.O., Adams, M.A., Turner, N.C., Beverly, C.R., Ong, C.K., Khan, A.A.H.,  
958 Bleby, T.M., 2001. An improved heat pulse method to measure low and reverse rates of  
959 sap flow in woody plants. *Tree Physiol.* 21, 589-598.

960 Cabon, A., Mouillot, F., Lempereur, M., Ourcival, J.M., Simioni, G., Limousin, J.M.,  
961 2018. Thinning increases tree growth by delaying drought-induced growth cessation in  
962 a Mediterranean evergreen oak coppice. *For. Ecol. Manage.* 409, 333-342.

963 Camarero, J.J., Sanguesa-Barreda, G., Vergarechea, M., 2016. Prior height, growth, and  
964 wood anatomy differently predispose to drought induced dieback in two Mediterranean  
965 oak species. *Ann. For. Sci.* 73, 341-351.

966 Chen, L., Zhang, Z., Zeppel, M., Liu, C., Guo, J., Zhu, J., Zhang, X., Zhang, J., Zha, T.,  
967 2014. Response of transpiration to rain pulses for two tree species in a semiarid  
968 plantation. *Int. J. Biometeorol.* 58, 1569–1581. doi: 10.1007/s00484-013-0761-9

969 Cotillas, M. Sabaté, S., Gracia, C., Espelta, J.M., 2009. Growth response of mixed  
970 mediterranean oak coppices to rainfall reduction. Could selective thinning have any  
971 influence on it? *For. Ecol. Manage.* 258, 1677–1683. doi:10.1016/j.foreco.2009.07.033

972 del Campo, A.D., Fernandes, T.J.G., Molina, A.J., 2014. Hydrology-oriented (adaptive)  
973 silviculture in a semiarid pine plantation: How much can be modified the water cycle  
974 through forest management? *Eur. J. Forest. Res.*, 133(5), 879-894.

975 del Campo, A.D., González-Sanchis, M., Lidón, A., Ceacero, C.J., García-Prats, A.,  
976 2018. Rainfall partitioning after thinning in two low-biomass semiarid forests: impact of  
977 meteorological variables and forest structure on the effectiveness of water-oriented  
978 treatments. *Journal of Hydrology*. Accepted.

979 Delzon, S., Sartore, M., Granier, A., Loustau, D., 2004. Radial profiles of sap flow with  
980 increasing tree size in maritime pine. *Tree Physiol.* 24, 1285–1293.

981 Delzon, S., Urli, M., Samalens, J.C., Lamy, J.B., Lischke, H., Sin, F., Zimmermann,  
982 N.E., Porté, A.J., 2013. Field evidence of colonisation by Holm Oak, at the northern

983 margin of its distribution range, during the anthropocene period. PLoS ONE 8(11),  
984 e80443. doi: 10.1371/journal.pone.0080443

985 Detty, J. M., McGuire, K. J., 2010. Topographical controls on shallow groundwater  
986 dynamics: implications of hydrologic connectivity between hillslopes and riparian zones  
987 in a till mantled catchment. *Hydrol. Process.* 24, 2222-2236. doi:10.1002/hyp.7656.

988 di Prima, S., Bagarello, V., Angulo-Jaramillo, R., Bautista, I., Cerdà, A., del Campo, A.,  
989 González-Sanchis, M., Iovino, M., Lassabatere, L., Maetzke, F. 2017. Impacts of  
990 thinning of a Mediterranean oak forest on soil properties influencing water infiltration.  
991 *J. Hydrol. Hydromech.*, 65, 3, 276–286.

992 Doblas-Miranda, E., Alonso, R., Arnan, X., Bermejo, V., Brotons, L., de las Heras, J.,  
993 Estiarte, M., Hódar, J.A., Llorens, P., Lloret, F., López-Serrano, F.R., Martínez-Vilalta,  
994 J., Moya, D., Peñuelas, J., Pino, J., Rodrigo, A., Roura-Pascual, N., Valladares, F., Vilà,  
995 M., Zamora, R., Retana, J., 2017. A review of the combination among global change  
996 factors in forests, shrublands and pastures of the Mediterranean Region: Beyond  
997 drought effects. *Glob. Planet. Change* 148, 42-54.

998 Domingo, F., Villagarcía, L., Brenner, A. J., Puigdefábregas, J., 2000. Measuring and  
999 modelling the radiation balance of a heterogeneous shrubland. *Plant Cell Environ.* 23,  
1000 27–38. doi:10.1046/j.1365-3040.2000.00532.x

1001 Ewers, B.E., Gower, S.T., Bond-Lamberty, B., Wang, C.K., 2005. Effects of stand age  
1002 and tree species on canopy transpiration and average stomatal conductance of boreal  
1003 forests. *Plant Cell Environ.* 28, 660–678.

1004 Ewers, B.E., Oren R., 2000. Analyses of assumptions and errors in the calculation of  
1005 stomatal conductance from sap flux measurements. *Tree Physiol.* 20(9), 579-589.

1006 Fernandes, T.J.G., del Campo, A.D., García-Bartual, R., González-Sanchis, M., 2015.  
1007 Coupling daily transpiration modelling with forest management in a semiarid pine  
1008 plantation. *iForest* 9, 38-48. doi: 10.3832/ifor1290-008

1009 Fernandes, T. J., del Campo, A. D., Herrera, R., Molina, A. J., 2016. Simultaneous  
1010 assessment, through sap flow and stable isotopes, of water use efficiency (WUE) in  
1011 thinned pines shows improvement in growth, tree-climate sensitivity and WUE, but not  
1012 in WUEi. *For. Ecol. Manag.* 361, 298-308.

1013 Flury M., Mathison J.B., Wu J.Q., Schillinger W.F., Stöckle C.O., 2009. Water vapor  
1014 diffusion through wheat straw residue. *Soil Sci. Soc. Am. J.* 73, 37-45.

1015 Fuchs, M., Hadas, A., 2011. Mulch resistance to water vapor transport. *Agric. Water*  
1016 *Manage.* 98 (6), 990-998

1017 Galiano, L., Martínez-Vilalta, J., Sabaté, S., Lloret, F. 2012. Determinants of drought  
1018 effects on crown condition and their relationship with depletion of carbon reserves in a  
1019 Mediterranean holm oak forest. *Tree Physiol.* 32 (4), 478–489  
1020 doi:10.1093/treephys/tps025.

1021 García de la Serrana, R., Vilagrosa, A., Alloza, J. A., 2015. Pine mortality in southeast  
1022 Spain after an extreme dry and warm year: interactions among drought stress,  
1023 carbohydrates and bark beetle attack. *Trees* 29, 1791-1804.

1024 Gea-Izquierdo, G., Martín-Benito, D., Cherubini, P., Cañellas, I., 2009. Climate-growth  
1025 variability in *Quercus ilex* L. west Iberian open woodlands of different stand density.  
1026 *Ann. For. Sci.* 66, 802. doi: 10.1051/forest/2009080

1027 Gentilesca, T., Camarero, J.J., Colangelo, M., Nolè, A., Ripullone, F., 2017. Drought-

1028 induced oak decline in the western Mediterranean region: an overview on current  
1029 evidences, mechanisms and management options to improve forest resilience. *iForest* 10  
1030 (5), 796-806. doi: 10.3832/ifor2317-010

1031 Girard, F., Vennetier, M., Ourmim, S., Caraglio, Y., Misson, L., 2011. Polycyclism, a  
1032 fundamental tree growth process, decline with recent climate change: the example of  
1033 *Pinus halepensis* Mill. in Mediterranean France. *Trees* 25, 311–322.

1034 Gracia, C.A., Sabaté, S., Martínez, J.M., Albeza, E., 1999. Functional responses to  
1035 thinning, in: Rodà, F., Retana, J., Gracia, C.A., Bellot, J. (Eds.), *Ecological Studies*,  
1036 137. Ecology of Mediterranean Evergreen Oak Forests. Springer, Berlin, pp. 329–338.

1037 Granier, A., 1987. Sap flow measurements in Douglas fir tree trunks by means of a new  
1038 thermal method. *Ann. For. Sci.* 44(1), 1–14.

1039 Granier, A., Biron, P., Köstner, B., Gay, L.W., Najjar, G., 1996. Comparisons of xylem  
1040 sap flow and water vapour flux at the stand level and derivation of canopy conductance  
1041 for Scots pine. *Theor. Appl. Climat.* 53, 115–122.

1042 Granier, A., Biron, P., Lemoine, D., 2000. Water balance, transpiration and canopy  
1043 conductance in two beech stands. *Agric. For. Meteorol.* 100, 291-308.

1044 Granier, A., Breda, N., 1996. Modelling canopy conductance and stand transpiration of  
1045 an oak forest from sap flow measurements. *Ann. For. Sci.* 53(2-3), 537-546.

1046 Grant, G.E., Tague, C.L., Allen, C.D., 2013. Watering the forest for the trees: an  
1047 emerging priority for managing water in forest landscapes. *Front. Ecol. Environ.* 11(6),  
1048 314–321. doi:10.1890/120209

1049 Gratani, L., Meneghini, M., Pesoli, P., Crescente, M.F., 2003. Structural and functional

1050 plasticity of *Quercus ilex* seedlings of different provenances in Italy. *Trees* 17, 515-52.

1051 Grossiord, C., Sevanto, S., Borrego, I., Chan, A. M., Collins, A. D., Dickman, L. T.,  
1052 Hudson, P. J., McBranch, N., Michaletz, S. T., Pockman, W. T., Ryan, M., Vilagrosa,  
1053 A., McDowell, N. G., 2017. Tree water dynamics in a drying and warming world. *Plant*  
1054 *Cell Environ.* 40, 1861–1873. doi: 10.1111/pce.12991.

1055 Hampe, A., Petit, R.J., 2005. Conserving biodiversity under climate change: the rear  
1056 edge matters. *Ecol. Lett.* 8, 461–67.

1057 Hatton, T.J., Catchpole, E.A., Vertessy, R.A., 1990. Integration of sapflow velocity to  
1058 estimate plant water use. *Tree Physiol.* 6, 201–209.

1059 Idso, S. B., 1981. A set of equations for full spectrum and 8- to 14- $\mu$ m and 10.5- to  
1060 12.5- $\mu$ m thermal radiation from cloudless skies. *Water Resour. Res.* 17(2), 295–304.  
1061 doi:10.1029/WR017i002p00295.

1062 Ilstedt, U., Bargués Tobella, A., Bazié, H.R., Bayala, J., Verbeeten, E., Nyberg, G.,  
1063 Sanou, J., Benegas, L., Murdiyarso, D., Laudon, H., Sheil, D., Malmer, A., 2016.  
1064 Intermediate tree cover can maximize groundwater recharge in the seasonally dry  
1065 tropics. *Sci. Rep.* 6, 21930, 1-12. doi:10.1038/srep21930

1066 Infante, J., Domingo, F., Fernández-Alés, R., Joffre, R., Rambal, S., 2003. *Quercus*  
1067 *ilex* transpiration as affected by a prolonged drought period. *Biol. Plantarum*, 46(1), 49-  
1068 55. <https://doi.org/10.1023/A:1022353915578>

1069 Jarvis, P.G., McNaughton, K.G., 1986. Stomatal control of transpiration: Scaling up  
1070 from leaf to region. *Adv. Ecol. Res.* 15, 1–49.

1071 Klein, T., Shpringer, I., Fikler, B., Elbaz, G., Cohen, S., Yakir, Y., 2013. Relationships

1072 between stomatal regulation, water-use, and water-use efficiency of two coexisting key  
1073 Mediterranean tree species. *For. Ecol. Manag.* 302, 34–42.

1074 Leblanc, S.G., Chen, J. M., 2001. A practical scheme for correcting multiple scattering  
1075 effects on optical LAI measurements. *Agric. Forest Meteorol.* 110, 125– 139.

1076 Lhomme, J. P., Montes, C., 2014. Generalized combination equations for canopy  
1077 evaporation under dry and wet conditions. *Hydrol. Earth Syst. Sci.* 18, 1137-1149.  
1078 <https://doi.org/10.5194/hess-18-1137-2014>, 2014.

1079 Lhomme, J. P., Montes, C., Jacob, F., Prévot, L., 2012. Evaporation from heterogeneous  
1080 and sparse canopies: on the formulations related to multi-source representations.  
1081 *Boundary Layer Meteorol.* 144, 243–262. <https://doi.org/10.1007/s10546-012-9713-x>

1082 Lhomme J.P., Rocheteau, A., Ourcival, J.M., Rambal, S., 2001. Nonsteady-state  
1083 modelling of water transfer in a Mediterranean evergreen canopy. *Agric. Forest*  
1084 *Meteorol.* 108, 67–83.

1085 Limousin, J.M., Rambal, S., Ourcival, J.M., Joffre, R., 2008. Modelling rainfall  
1086 interception in a mediterranean *Quercus ilex* ecosystem: Lesson from a throughfall  
1087 exclusion experiment. *J. Hydrol.* 357, 57-66.

1088 Limousin, J.M., Rambal, S., Ourcival, J.M., Rocheteau, A., Joffre, R., Rodriguez-  
1089 Cortinta, R., 2009. Long-term transpiration change with rainfall decline in a  
1090 Mediterranean *Quercus ilex* forest. *Glob. Change Biol.* 15, 2163–2175.

1091 Lindner, M., Fitzgerald, J. B., Zimmermann, N., Reyer, C., Delzon, S., van der Maaten,  
1092 E., Schelhaas, M. J., Lasch, P., Eggers, J., van der Maaten-Theunissen, M., Suckow, F.  
1093 Psomas, A., Poulter, B., Hanewinkel, M., 2014. Climate change and European forests:

1094 what do we know, what are the uncertainties, and what are the implications for forest  
1095 management? *J. Environ. Manage.* 146, 69-83.

1096 López, B.C., Sabaté, S., Gracia, C.A., 1998. Fine roots dynamics in a Mediterranean  
1097 forest: effects of drought and stem density. *Tree Physiol.* 18, 601–606.

1098 López, B.C., Sabaté, S., Gracia, C.A., 2003. Thinning effects on carbon allocation to  
1099 fine roots in a *Quercus ilex* forest. *Tree Physiol.* 23, 1217–1224.

1100 Martínez-Ferri, E., Balaguer, L., Valladares, F., Chico, J.M., Manrique, E., 2000.  
1101 Energy dissipation in drought-avoiding and drought-tolerant tree species at midday  
1102 during the Mediterranean summer. *Tree Physiol.* 20, 131–138.

1103 Martínez-Vilalta, J., Mangirón, M., Ogaya, R., Sauret, M., Serrano, L., Peñuelas, J.,  
1104 Piñol, J., 2003. Sap flow of three co-occurring Mediterranean woody species under  
1105 varying atmospheric and soil water conditions. *Tree Physiol.* 23, 747–758.

1106 Mayor, X., Rodà, F., 1993. Growth response of holm oak (*Quercus ilex* L) to  
1107 commercial thinning in the Montseny mountains (NE Spain). *Ann. For. Sci.* 50, 247-  
1108 256.

1109 Monteith, J.L., Unsworth, M., 1990. Principles of environmental physics. Butterworth-  
1110 Heinemann, 2nd edition. Burlington-MA, 304 pages.

1111 Molina, A., del Campo, A.D., 2012. The effects of experimental thinning on throughfall  
1112 and stemflow: a contribution towards hydrology-oriented silviculture in Aleppo pine  
1113 plantations. *For. Ecol. Manage.* 269, 206–213.

1114 Moreno, G., Cubera, E., 2008. Impact of stand density on water status and leaf gas  
1115 exchange in *Quercus ilex*. *For. Ecol. Manage.* 254, 74–84.

1116 doi:10.1016/j.foreco.2007.07.029

1117 Novick, K.A., Ficklin, D.L., Stoy, P.C., Williams, C.A., Bohrer, G., Oishi, A.C.,  
1118 Papuga, S.A., Blanken, P.D., Noormets, A., Sulman, B.N., Scott, R.L., Wang, L.,  
1119 Phillips, R.P., 2016. The increasing importance of atmospheric demand for ecosystem  
1120 water and carbon fluxes. *Nat. Clim. Change* 6(11), 1023-1027. doi:  
1121 10.1038/nclimate3114

1122 Olivar, J., Bogino, S., Rathgeber, C., Bonnesoeur, V., Bravo, F., 2014. Thinning has a  
1123 positive effect on growth dynamics and growth–climate relationships in Aleppo pine  
1124 (*Pinus halepensis*) trees of different crown classes. *Ann. For. Sci.* 71, 395–404. doi:  
1125 10.1007/s13595-013-0348-y

1126 Oren, R., Sperry, J.S., Katul, G.G., Pataki, D.E., Ewers, B.E., Phillips, N., Schäfer,  
1127 K.V.R., 1999. Intra- and interspecific responses of canopy stomatal conductance to  
1128 vapour pressure deficit. *Plant Cell Environ.* 22, 1515–1526.

1129 Peñuelas, J., Sardans, J., Filella, I., Estiarte, M., Llusà, J., Ogaya, R., Carnicer, J.,  
1130 Bartrons, M., Rivas-Ubach, A., Grau, O., Peguero, G., Margalef, O., Pla-Rabés, S.,  
1131 Stefanescu, C., Asensio, D., Preece, C., Liu, L., Verger, A., Rico, L., Barbeta, A.,  
1132 Achotegui-Castells, A., Gargallo-Garriga, A., Sperlich, D., Farré-Armengol, G.,  
1133 Fernández-Martínez, M., Liu, D., Zhang, C., Urbina, I., Camino, M., Vives, M., Nadal-  
1134 Sala, D., Sabaté, S., Gracia, C., Terradas, J., 2017. Assessment of the impacts of climate  
1135 change on Mediterranean terrestrial ecosystems based on data from field experiments  
1136 and long-term monitored field gradients in Catalonia. *Environ. Exp. Bot.*,  
1137 <https://doi.org/10.1016/j.envexpbot.2017.05.012>

1138 Pérez- Cueva, A.J., 1994. Atlas climático de la Comunidad Valenciana. COPUT,

1139 Generalitat Valenciana.

1140 Perry, T. D., Jones, J. A., 2016. Summer streamflow deficits from regenerating  
1141 Douglas-fir forest in the Pacific Northwest, USA. *Ecohydrology*,  
1142 <https://doi.org/10.1002/eco.1790>

1143 Prober, S.M., Byrne, M., McLean, E.H., Steane, D.A., Potts, B.M., Vaillancourt, R.E.,  
1144 Stock, W.D., 2015. Climate-adjusted provenancing: a strategy for climate-resilient  
1145 ecological restoration. *Front. Ecol. Evol.* 3, 65, 1-8. doi: 10.3389/fevo.2015.00065

1146 RStudio Team, 2015. RStudio: Integrated Development for R. RStudio, Inc., Boston,  
1147 MA URL <http://www.rstudio.com/>.

1148 Raz Yaseef, N., Rotenberg, E., Yakir, D., 2010a. Effects of spatial variations in soil  
1149 evaporation caused by tree shading on water flux partitioning in a semi-arid pine forest.  
1150 *Agric. For. Meteorol.* 150, 454–462.

1151 Raz Yaseef, N., Yakir, D., Rotenberg, E., Schiller, G., Cohen, S., 2010b. *Ecohydrology*  
1152 of a semi-arid forest: partitioning among water balance components and its implications  
1153 for predicted precipitation changes. *Ecohydrology* 3, 143–154.

1154 Reyes-Acosta, L. J., Lubczynski, M. W., 2013. Mapping dry-season tree transpiration of  
1155 an oak woodland at the catchment scale, using object-attributes derived from satellite  
1156 imagery and sap flow measurements. *Agric. For. Meteorol.* 174-175, 184–201.

1157 Rubio, E., Caselles, V., Badenas, C., 1997. Emissivity measurements of several soils  
1158 and vegetation types in the 8-14 mm waveband: analysis of two field methods. *Remote*  
1159 *Sens. Environ.* 59, 490–521.

1160 Ruiz de la Torre J., 2006. *Flora Mayor*. Organismo Autónomo Parques Nacionales.

- 1161 Dirección General para la Biodiversidad, Madrid. pp. 1293-1295.
- 1162 Seidl, R., Spies, T. A., Peterson, D. L., Stephens, S. L., Hicke, J. A., 2016. Searching  
1163 for resilience: addressing the impacts of changing disturbance regimes on forest  
1164 ecosystem services. *J. Appl. Ecol.* 53, 120–129.
- 1165 Shaw, R. H., Pereira, A. R., 1982. Aerodynamic roughness of a plant canopy: a  
1166 numerical experiment. *Agric. Meteorol.* 26, 51–65.
- 1167 Shuttleworth, W.J., Wallace, J.S., 1985. Evaporation from sparse crops-an energy  
1168 combination theory. *Q J R Meteorol. Soc.* 111, 839–855.
- 1169 Stahl, U., Reu, B., Wirth, C., 2014. Predicting species' range limits from functional  
1170 traits for the tree flora of North America. *PNAS* 111 (38), 13739-13744.  
1171 doi:10.1073/pnas.1300673111
- 1172 Terradas, J., 1999. Holm oak and Holm oak forests: an introduction. In: Rodá, F.,  
1173 Retana, J., Gracia, C.A., Bellot, J. (Eds.), *Ecological Studies*, 137. Ecology of  
1174 Mediterranean Evergreen Oak Forests. Springer, Berlin, pp. 1–14.
- 1175 Terradas, J., Savè, R., 1992. The influence of summer and winter water relationships on  
1176 the distribution of *Quercus ilex* L. *Vegetatio*, 99(100), 137-145.
- 1177 Thornthwaite, C. W., 1948. An approach toward a rational classification of climate.  
1178 *Geographical Review*, 38(1), 55–94.
- 1179 Trifilò, P., Nardini, A., Lo Gullo, M.A., Barbera, P.M., Savi, T., Raimondo F., 2015.  
1180 Diurnal changes in embolism rate in nine dry forest trees: relationships with species-  
1181 specific xylem vulnerability, hydraulic strategy and wood traits. *Tree Physiol.* 35, 694–  
1182 705. doi:10.1093/treephys/tpv049

- 1183 Ungar, E.D., Rotenberg, E., Raz-Yaseef, N., Cohen, S., Yakir, D., Schiller, G., 2013.  
 1184 Transpiration and annual water balance of Aleppo pine in a semiarid region:  
 1185 implications for forest management. *For. Ecol. Manag.* 298, 39–51.
- 1186 Valero-Galván, J., Valledor, L., Navarro-Cerrillo, R.M., Gil-Pelegrián, E., Jorrín-Novo,  
 1187 J.V., 2011. Studies of variability in Holm oak (*Quercus ilex* subsp. *ballota* [Desf.]  
 1188 Samp.) through acorn protein profile analysis. *J. Proteomics* 74(8), 1244-55. doi:  
 1189 10.1016/j.jprot.2011.05.003.
- 1190 Wang, W., 2014. Analytically Modelling Mean Wind and Stress Profiles in Canopies  
 1191 *Boundary-Layer Meteorol* 151, 239–256 doi: 10.1007/s10546-013-9899-6
- 1192 Wright, I.J., Reich, P.B., Westoby, M., Ackerly, D.D., Baruch, Z., Bongers, F., 2004.  
 1193 The worldwide leaf economics spectrum. *Nature* 428, 821–827.  
 1194 doi:10.1038/nature02403
- 1195 Zhang, B., Kang, S., Li, F., Zhang, L., 2008. Comparison of three evapotranspiration  
 1196 models to Bowen ratio-energy balance method for a vineyard in an arid desert region of  
 1197 northwest China. *Agricultural and Forest Meteorology* 148, 1629 – 1640. doi:  
 1198 10.1016/j.agrformet.2008.05.016

1199

1200 TABLE CAPTIONS

1201 **Table 1.** Biometric and inventory variables of holm oaks in the control and treated  
 1202 plots. C: control; T: Treated; BA: basal area;  $D_B$ : basal diameter;  $D_{BH}$ : diameter at  
 1203 breast height; De: density. See text for intervals of diameter classes. The frequency of  
 1204 diameter classes between both inventories is assumed to be constant even though there

1205 was a slight variation between the dates for the two. Only trees/stems higher than 1.5 m  
1206 were inventoried; lower heights were considered as shrubs. All tree groups integrate  
1207 interspersed trees of *Pinus halepensis*, *Juniperus sp.* and *Quercus faginea*.

1208 **Table 2.** Mean annual values of the growth variables after the clearing treatment for  
1209 both the control and the cleared plots. Bold font indicates significant ( $p \leq 0.05$ )  
1210 differences between control and treatment. The column on the right gives the values of  
1211 the same variables for the epicormic shoots and stump sprouts observed in the thinned  
1212 plot.

1213 **Table 3.** Significant correlations ( $p \leq 0.01$ ,  $p \leq 0.05$  in italic font) between tree  
1214 transpiration (sap flow velocity, vs,  $\text{cm h}^{-1}$ ; and sap flow, Sf,  $\text{L tree}^{-1} \text{h}^{-1}$ ) and the  
1215 explanatory variables related to date, atmosphere, soil moisture, tree structure and  
1216 cultural treatment at different temporal scales (hourly, daily and seasonal) either for the  
1217 entire study period or in the growing season (Mar-Oct) within daylight hours (11 am – 4  
1218 pm, only at the hourly time step); blank cells: non-significant correlation. Shaded cells:  
1219 not applicable. Year: 2012-2016, MJD: Modified Julian Date, D: vapor pressure deficit  
1220 (kPa), U: wind speed ( $\text{m s}^{-1}$ ),  $R_{s,a}$ : Solar radiation ( $\text{W m}^{-2}$ ), T: Temperature ( $^{\circ}\text{C}$ ),  $\theta_{\text{rel}}$ :  
1221 relative soil moisture content at 15 cm (%), Treatment: Clearing treatment (C,T), DC:  
1222 diameter class (1-2, 3-4), DBH: diameter breast height (cm), Sa: tree sapwood area  
1223 ( $\text{cm}^2$ ), Cpa: tree crown projected area ( $\text{m}^2$ ). N varied between 50 and 315,000,  
1224 depending on the scale.

1225 **Table 4.** Importance of the independent variables (sorted by date, atmosphere, soil  
1226 moisture, tree structure and culture treatment) in the variance explained by the MLR  
1227 models fitted for tree transpiration (vs,  $\text{cm h}^{-1}$  and Sf,  $\text{L tree}^{-1} \text{h}^{-1}$ ). Importance, a  
1228 relative term from 0 to 100, was computed as the contribution of each specific variable  
1229 to the sum of squares in the fitted models (totals for each sorted class are given). In all

1230 cases, data were filtered by growing season (Mar-Oct) and by daylight hours (11 am – 4  
1231 pm) in the hourly step analyses. Full models are available in Supplementary Material.  
1232 **Table 5.** Partitioning of annual dry-canopy evapotranspiration, ET (mm and % of Pg) in  
1233 the control plot (C) and the cleared plot (T). Pg: gross rainfall;  $E_t$ : stand transpiration;  
1234  $E_s$ : evaporation from soil,  $E_r$ : residual term including transpiration from grass/shrub.

1235

## 1236 FIGURE CAPTIONS

1237 **Figure 1.** Progression of environmental and climatic variables during the study period:  
1238 cumulative precipitation (annual P, cm, gray staked area), daily precipitation (P, mm,  
1239 bars), daily mean solar radiation ( $R_{s,a}$ ,  $W\ m^{-2}$ ), daily mean air temperature (T, °C), daily  
1240 mean vapor pressure deficit (D, hPa). Daily mean relative soil water content at 15 cm in  
1241 both plots (treatments) is also plotted.

1242 **Figure 2.** Mean annual values of the growth variables in both the control (C) and the  
1243 thinned (T) plots in the suppressed-intermediate trees (diameter classes 1 and 2) and the  
1244 dominant-codominant trees (diameter classes 3 and 4). Asterisk indicates significant  
1245 ( $p \leq 0.05$ ) differences between control and treatment regardless of the diameter class.

1246 **Figure 3.** Seasonal values of LAI in both the control (C) and the cleared (T) plots  
1247 measured at 0.5 m above ground. From mid-2015 on, resprouting became more  
1248 important in the cleared plot and prevented the summer drop in 2016, surpassing the  
1249 value of the control plot by the end of the study. Linear trend lines are given in each  
1250 series. Dashed line represents the series of the MODIS LAI product averaged by month.

1251 **Figure 4.** Box and whiskers plots for sap flow velocity and sap flow in control (C) and  
1252 cleared (T) trees in both the suppressed-intermediate trees (diameter classes 1 and 2)  
1253 and the dominant-codominant trees (diameter classes 3 and 4). Plots are given for either  
1254 the entire study period (left) or the growing season period (right, March to October,

1255 both included). Black dots and figures represent the mean value. Whiskers are for the  
1256 5th and 95th percentiles.

1257 **Figure 5.** Influence of vapor pressure deficit (D) on simultaneous canopy conductance  
1258 ( $G_s$ ) on an hourly basis after applying boundary line analysis in the control plot (black  
1259 circles and lines) and the thinned plot (gray triangles and lines) under different relative  
1260 soil water conditions ( $\theta_{rel}$ ). Both the absolute and the  $\ln$  values of D (with constant slope  
1261 over the entire range of D) are shown.

1262 **Figure 6.** Relationship between  $m$  ( $G_s$  sensitivity to D) and  $G_{sref}$  under different relative  
1263 soil moisture conditions ( $\theta_{rel}$ ) in the control plot (black circles) and the thinned plot  
1264 (gray triangles). The two bottom plots represent the individual variation of either  $m$  or  
1265  $G_{sref}$  for the soil moisture classes defined. The gray line represents the theoretical  
1266 proportionality of 0.6 described.

1267 **Figure 7.** Mean daily values of the different components of dry-canopy  
1268 Evapotranspiration in both plots (C and T) sorted by year. Es: soil evaporation; Et: oak  
1269 transpiration; Er: residual evaporation. Values are shown for both the entire year and the  
1270 growing season (March to October, both included). Data in 2012 were from October 1<sup>st</sup>  
1271 onwards.

1272 **Figure 8.** Progression of the different components of evapotranspiration (ET) in both  
1273 plots (control: C and treatment: T) during the study period: Es: soil evaporation; Et: oak  
1274 transpiration. In soil evaporation and canopy transpiration the relative soil water content  
1275 (0-1) at 5 and 30 cm is provided for C and T plots, respectively.

1276 **Figure 9.** Seasonal progression of the daily ratio  $\ln(\text{Treated}/\text{Control})$  of ET and its three  
1277 components (below) and the concomitant values of annual cumulative  $P_g$  (shaded area)  
1278 and total ET plus  $E_i$  (dry plus wet canopy) (above) (see text for details). Baseline of the  
1279 logarithmic ratio before treatment is assumed to be zero. Daily precipitation (black bars)

1280 is also reproduced here. In 2012, ET in both C and T was arbitrarily assigned to begin at  
 1281 115 mm. The  $E_r$  line represents 9 days running average.

1282

1283 **Table 1.**

Plot	Date	D <sub>B</sub> cm	D <sub>BH</sub> cm	De trees ha <sup>-1</sup> (oaks/all trees)	BA m <sup>2</sup> ha <sup>-1</sup>	Diameter class (DC)			
						1	2	3	4
						Basal area (m <sup>2</sup> ha <sup>-1</sup> )			
C,T	2012- Before Treatment	10.7	7.7	1059/1133	5.60	0.27	0.55	1.67	3.10
T	2012- After Treatment	16.0	12.3	289/317	2.82	0.07	0.24	0.50	2.01
C	2016	11.6	8.4	1059/1133	8.31	1.03	1.35	2.62	3.66
T	2016	17.1	13.3	289/317	5.14	0.06	0.50	0.91	3.67
						Frequency (0-1)			
C	2012-16					0.531	0.182	0.175	0.112
T	2012-16					0.154	0.269	0.231	0.346

1284

1285 **Table 2.**

	Control (C)	Treated (T)	F, Chi	Treatment: epicormic and stump shoots
Shoot length (cm)	4.3±2.3	4.4±2.5	(ns)	13.4±4.0
Shoot diameter (mm)	1.69±0.44	1.81±0.71	(ns)	2.74±0.37
Shoot leaves (n <sup>o</sup> )	<b>6.4±3.8</b>	<b>7.3±3.7</b>	(*)	18.8±4
Shoot leaf area (cm <sup>2</sup> )	<b>32.3±20.2</b>	<b>28.8±16.9</b>	(*)	79.5±23.1
Shoot SLA (cm <sup>2</sup> mg <sup>-1</sup> )	<b>0.040±.002</b>	<b>0.042±.001</b>	(*)	0.045±.009
Shoots per branch (n <sup>o</sup> )	<b>34.9±13.3</b>	<b>49.4±30.5</b>	(*)	-
Tree-based LAI (m <sup>2</sup> m <sup>-2</sup> )	0.81±0.31	0.93±0.22	2.36 (ns)	-

1286

1287

1288

**Table 3.**

		Date		Atmosphere				$\theta_{rel}$	Treat ment	Tree size				
		Year	MJD	Hour	D	U	$R_{s,a}$			T	DC	$D_{BH}$	Sa	Cpa
Hourly time step														
Entire period	$v_s$	0.08	0.07	0.09	0.26	0.04	0.19	0.28	-0.17	0.17	0.08	0.05	0.06	0.06
	$S_f$	0.10	0.10	0.10	0.21	0.05	0.16	0.23	-0.12	0.19	0.22	0.38	0.44	0.44
Growing season	$v_s$	0.39	0.38	0.09	0.18	0.18	0.07	0.16	-0.08	0.25	0.18	0.20	0.20	0.17
	$S_f$	0.24	0.23	0.06	0.12	0.11	0.05	0.11	-0.07	0.24	0.28	0.57	0.61	0.60
Daily time step														
Entire period	$v_s$	0.13	0.12		0.43	-0.16	0.48	0.40	-0.29	0.29	0.08	0.15	0.16	0.13
	$S_f$	0.12	0.12		0.27	-0.08	0.27	0.25	-0.18	0.28	0.33	0.66	0.71	0.69
Growing season	$v_s$	0.10	0.08		0.30	-0.07	0.34	0.23	-0.16	0.35	0.09	0.18	0.18	0.15
	$S_f$	0.10	0.09		0.18	-0.02	0.18	0.15	-0.11	0.31	0.36	0.73	0.79	0.77
Vegetative period time step (Nov-Feb, Mar-Oct)														
Entire period	$v_s$	0.29			0.28		0.26	0.25	-0.23					
	$S_f$				0.34	-0.21	0.32	0.31	-0.27	0.29	0.35	0.69	0.74	0.72
Growing season	$v_s$	0.31			0.47		0.39	0.49		0.43				
	$S_f$									0.33	0.39	0.78	0.84	0.82

1289

1290

**Table 4.**

		Importance (0-100)				
	Adj. $r^2$	Date	Atmosphere	$\theta_{rel}$	Treatment	Tree structure
Hourly time step						
$v_s$	0.283 <sup>S,#</sup>	2.0	12.0	10.0	27.0	49.0
$S_f$	0.473 <sup>S,#</sup>	2.0	11.0	5.0	29.0	53.0
Daily time step						
$v_s$	0.343 <sup>#</sup>	9.9	9.6	0.8	25.6	53.9
$S_f$	0.711 <sup>#</sup>	10.4	13.9	0.7	26.8	48.1
Growing season (Mar-Oct)						
$v_s$	0.392	-	57.0	-	43.0	-

S <sub>f</sub>	0.774	-	9.0	-	2.0	89.0
----------------	-------	---	-----	---	-----	------

1291 \$ showed autocorrelation; # showed multi-collinearity.

1292

1293 **Table 5.**

Treatm ent	ET mm	E <sub>s</sub> mm	E <sub>t</sub> mm	E <sub>r</sub> mm	ET % Pg	E <sub>s</sub> % Pg	E <sub>t</sub> % Pg	E <sub>r</sub> % Pg
2012 (Oct-Dec) (Pg: 262 mm)								
C	19	3.5	11.5	4.0	7%	1%	4%	2%
T	18	7.0	8.0	3.1	7%	3%	3%	1%
2013 (Pg: 405 mm)								
C	138	45	77	16	34%	11%	19%	4%
T	154	81	58	15	38%	20%	14%	4%
2014 (Pg: 354 mm)								
C	171	51	108	12	48%	14%	31%	3%
T	208	89	101	18	59%	25%	29%	5%
2015 (Pg: 320 mm)								
C	201	49	105	46	63%	15%	33%	14%
T	251	86	121	44	78%	27%	38%	14%
2016 (Pg: 499 mm)								
C	156	43	87	25	31%	9%	17%	5%
T	176	64	94	18	35%	13%	19%	4%
Total 2013-2016 (Pg: 1578 mm)								
C	665	188	378	99	42%	12%	24%	6%
T	789	320	374	94	50%	20%	24%	6%

1294

1295

1296

## SUPPLEMENTAL MATERIAL

Table S1. Hourly MLR full models for sap flow

S1.a) Dependent Variable: Sap flow velocity ( $v_s$ ,  $\text{cm h}^{-1}$ )

R Square	Adjusted R Square	Std. Error of the Estimate	Durbin-Watson	F
.283	.283	2.624867001030	.383	1336.680***

	Unstandardized Coefficients		Standardized Coefficients	t	Sig.	Collinearity Statistics		Importance
	B	Std. Error	Beta			Tolerance	VIF	
(Constant)	-1989.132	23.486		-84.695	.000			
year	.983	.012	.381	84.392	.000	.798	1.253	2
Treat.	3.613	.098	.583	36.960	.000	.065	15.273	27
D	.000	.000	.096	9.392	.000	.155	6.460	1
DC	.072	.003	.239	25.703	.000	.189	5.293	13
$\theta_{rel\ 15}$	2.248	.091	.134	24.582	.000	.550	1.817	10
Sa	-.007	.001	-.364	-7.318	.000	.007	152.019	1
U <sub>av</sub>	.469	.033	.062	14.009	.000	.825	1.212	5
T	.036	.004	.092	8.563	.000	.141	7.114	2
BA	-.088	.003	-7.299	-25.177	.000	.000	5164.556	13
Cpa	1.065	.042	5.877	25.082	.000	.000	3371.358	13
D <sub>BH</sub>	.703	.032	1.774	22.181	.000	.003	392.938	10
R <sub>s,a</sub>	.001	.000	.051	9.780	.000	.598	1.673	2
Hour	.088	.010	.048	8.985	.000	.562	1.780	2

S1.b) Dependent Variable: Sap flow ( $S_f$ ,  $1 \text{ tree}^{-1} \text{ hour}^{-1}$ )

R Square	Adjusted R Square	Std. Error of the Estimate	Durbin-Watson	F
.473	.473	.889392744849	.318	3553.263***

	Unstandardized Coefficients		Standardized Coefficients	t	Sig.	Collinearity Statistics		Importance
	B	Std. Error	Beta			Tolerance	VIF	
(Constant)	-470.179	7.164		-65.635	.000			
Sa	.004	.000	.513	14.444	.000	.008	123.142	6.5
year	.233	.004	.230	65.412	.000	.828	1.207	1.8
D <sub>BH</sub>	.052	.009	.326	5.738	.000	.003	314.110	1
D	5.469E-5	.000	.050	6.153	.000	.154	6.479	0.4
Treat.	.746	.025	.304	30.384	.000	.102	9.799	28.7
$\theta_{rel\ 15}$	.390	.029	.059	13.458	.000	.538	1.858	5.1
DC	.020	.001	.178	25.587	.000	.212	4.717	20.4
Cpa	.246	.011	3.348	21.503	.000	.000	2365.037	14.4
BA	-.018	.001	-3.722	-18.665	.000	.000	3879.167	11
U <sub>av</sub>	.119	.010	.042	11.674	.000	.808	1.238	5
T	.012	.001	.078	9.048	.000	.137	7.281	2.6
Hour	.022	.003	.031	7.387	.000	.570	1.755	1.7
R <sub>s,a</sub>	.000	.000	.028	6.660	.000	.597	1.676	1.3

**Table S2.** Daily MLR full models for sap flow

S2.a) Dependent Variable: Sap flow velocity ( $v_s$ ,  $\text{cm h}^{-1}$ )

R Square	Adjusted R Square	Std. Error of the Estimate	Durbin-Watson	F
.344	.343	1.3990840	1.687	344.315***

	Unstandardized Coefficients		Standardized Coefficients	t	Sig.	Collinearity Statistics		Importance
	B	Std. Error	Beta			Tolerance	VIF	
(Constant)	-3172.947	199.397		-15.913	.000			
Treat.	3.582	.116	1.037	30.802	.000	.074	13.604	25.6
$R_{s,a}$	.004	.000	.184	14.905	.000	.549	1.822	5.5
D	.000	.000	.150	11.046	.000	.451	2.218	0.8
$D_{BH}$	.940	.038	4.243	24.498	.000	.003	359.815	16.2
$U_{av}$	-879	.070	-.126	-12.473	.000	.819	1.221	3.3
year	1.696	.107	1.169	15.796	.000	.015	65.712	5.3
MJD	-.004	.000	-1.113	-14.716	.000	.015	68.559	4.6
$\theta_{rel\ 15}$	-.718	.126	-.077	-5.696	.000	.453	2.209	0.8
BA	-.106	.004	-15.782	-25.293	.000	.000	4670.135	17.3
Cpa	1.217	.051	11.979	23.845	.000	.000	3027.480	15.4
DC	.045	.003	.273	12.903	.000	.187	5.352	4.5
Sa	-.005	.001	-.498	-4.488	.000	.007	147.481	0.5

S2.b) Dependent Variable: Sap flow ( $Sf$ ,  $l\ tree^{-1}\ hour^{-1}$ )

R Square	Adjusted R Square	Std. Error of the Estimate	Durbin-Watson	F
.712	.711	.3575846	1.664	1819.292***

	Unstandardized Coefficients		Standardized Coefficients	t	Sig.	Collinearity Statistics		Importance
	B	Std. Error	Beta			Tolerance	VIF	
(Constant)	-534.540	47.559		-11.239	.000			
Sa	.003	.000	.748	11.813	.000	.008	123.081	9.0
D	.000	.000	.106	12.415	.000	.449	2.227	2.9
$D_{BH}$	.036	.009	.413	4.079	.000	.003	314.032	1.1
Treat.	.485	.024	.364	20.371	.000	.102	9.803	26.7
$R_{s,a}$	.001	.000	.095	12.361	.000	.555	1.800	8.7
year	.283	.026	.514	11.065	.000	.015	66.075	6.2
DC	.012	.001	.194	15.642	.000	.212	4.713	15.8
Cpa	.154	.011	3.853	13.879	.000	.000	2363.815	12.4
BA	-.012	.001	-4.391	-12.352	.000	.000	3877.536	9.8
MJD	-.001	.000	-.431	-9.120	.000	.015	68.555	4.2
$U_{av}$	-.125	.017	-.048	-7.559	.000	.812	1.231	2.3
$\theta_{rel\ 15}$	-.108	.030	-.030	-3.552	.000	.453	2.206	0.7

**Table S3.** Seasonal MLR full models for sap flowS3.a) Dependent Variable: Sap flow velocity ( $v_s$ ,  $\text{cm h}^{-1}$ )

R Square	Adjusted R Square	Std. Error of the Estimate	Durbin-Watson	F
.418	.392	1.046155	2.293	16.131***

	Unstandardized Coefficients		Standardized Coefficients	t	Sig.	Collinearity Statistics		Importance
	B	Std. Error	Beta			Tolerance	VIF	
(Constant)	-4.919	1.528		-3.220	.002			
T	.426	.100	.486	4.271	.000	1.000	1.000	57
Treat.	1.131	.302	.426	3.744	.001	1.000	1.000	43

S3.b) Dependent Variable: Sap flow ( $Sf$ ,  $1 \text{ tree}^{-1} \text{ hour}^{-1}$ )

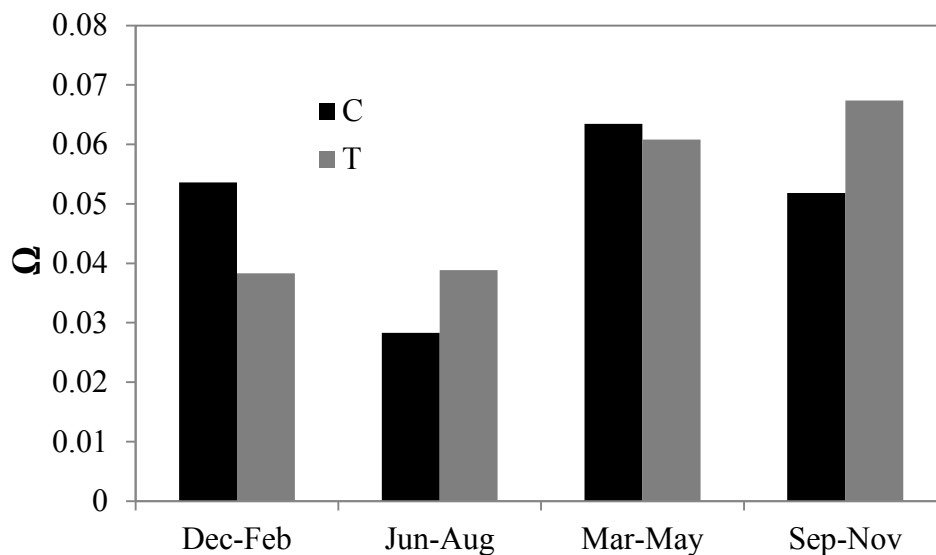
R Square	Adjusted R Square	Std. Error of the Estimate	Durbin-Watson	F
.788	.774	.266956	1.910	56.877***

	Unstandardized Coefficients		Standardized Coefficients	t	Sig.	Collinearity Statistics		Importance
	B	Std. Error	Beta			Tolerance	VIF	
(Constant)	-1.545	.390		-3.962	.000			
Treat.	.148	.078	.133	1.895	.064	.941	1.063	2
T	.093	.025	.248	3.650	.001	1.000	1.000	9
Sa	.003	.000	.810	11.566	.000	.941	1.063	89

**Figure S1.** Mean annual values of sap flow variables ( $V_s$ ,  $S_f$ ) and vapour pressure deficit ( $D$ , mean of daily maximums) in both the control (C) and the cleared (T) plots in the suppressed-intermediate trees (diameter classes 1 and 2) and the dominant-codominant trees (diameter classes 3 and 4).



**Figure S2.** Seasonal mean values of the decoupling coefficient  $\Omega$  in both the control (C) and the cleared (T) plots.



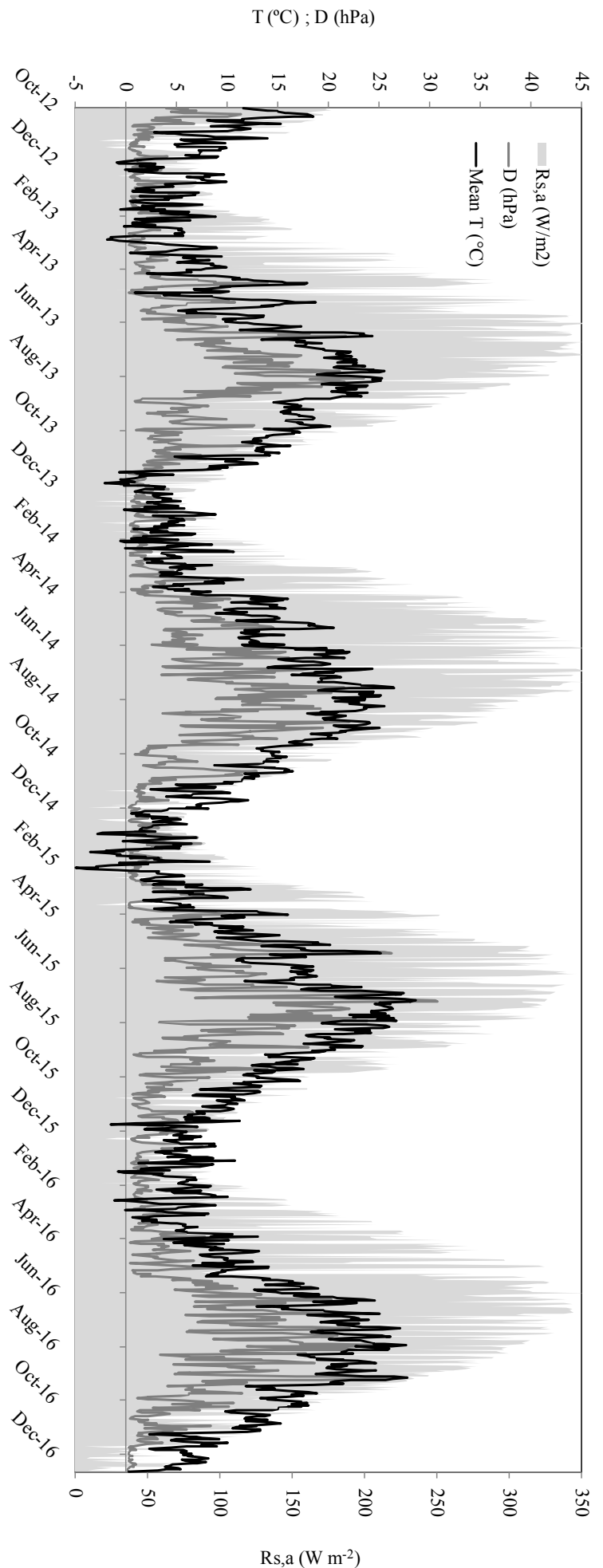
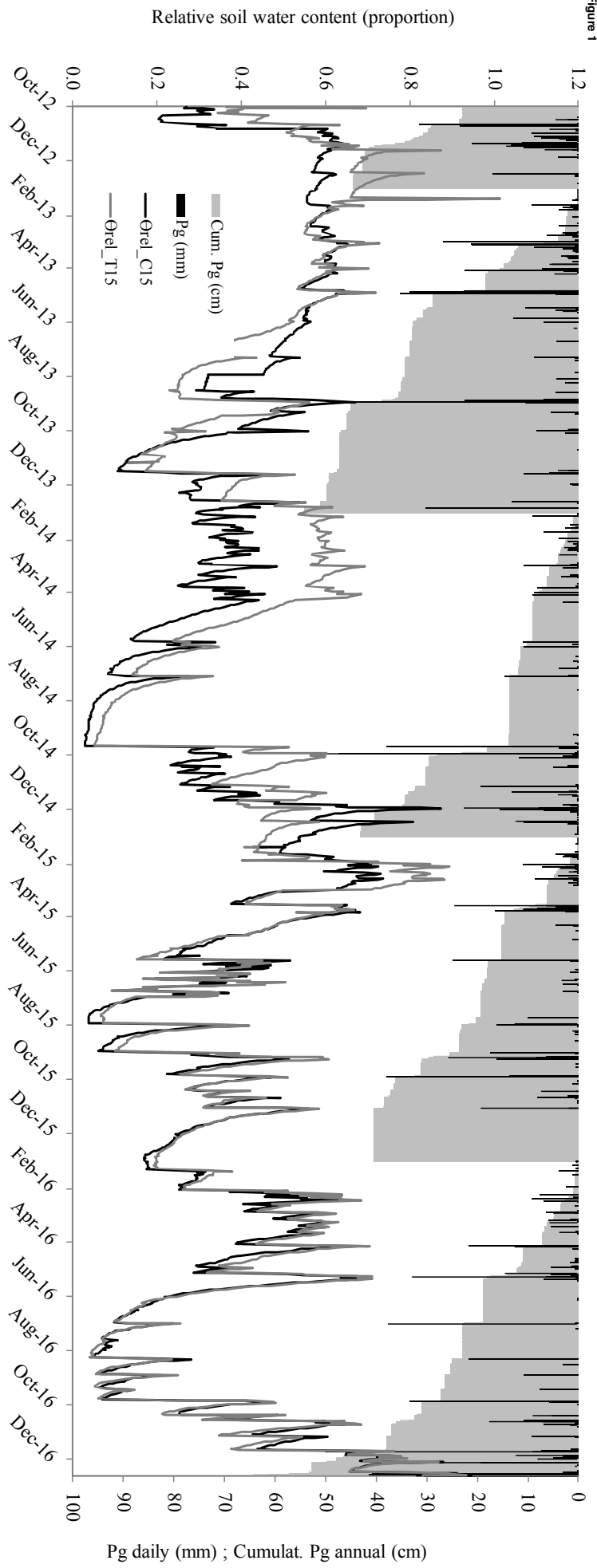


Figure 2

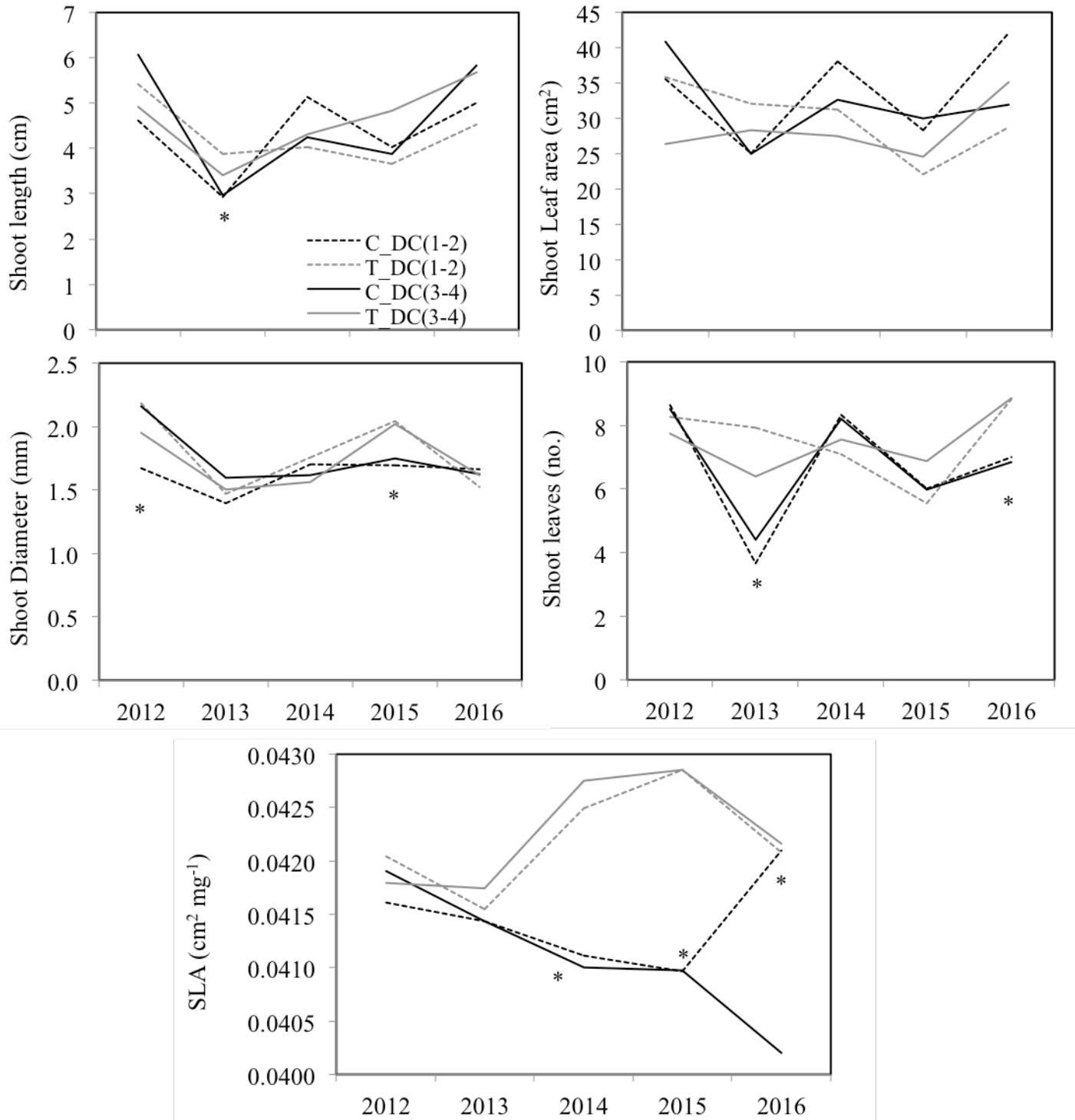
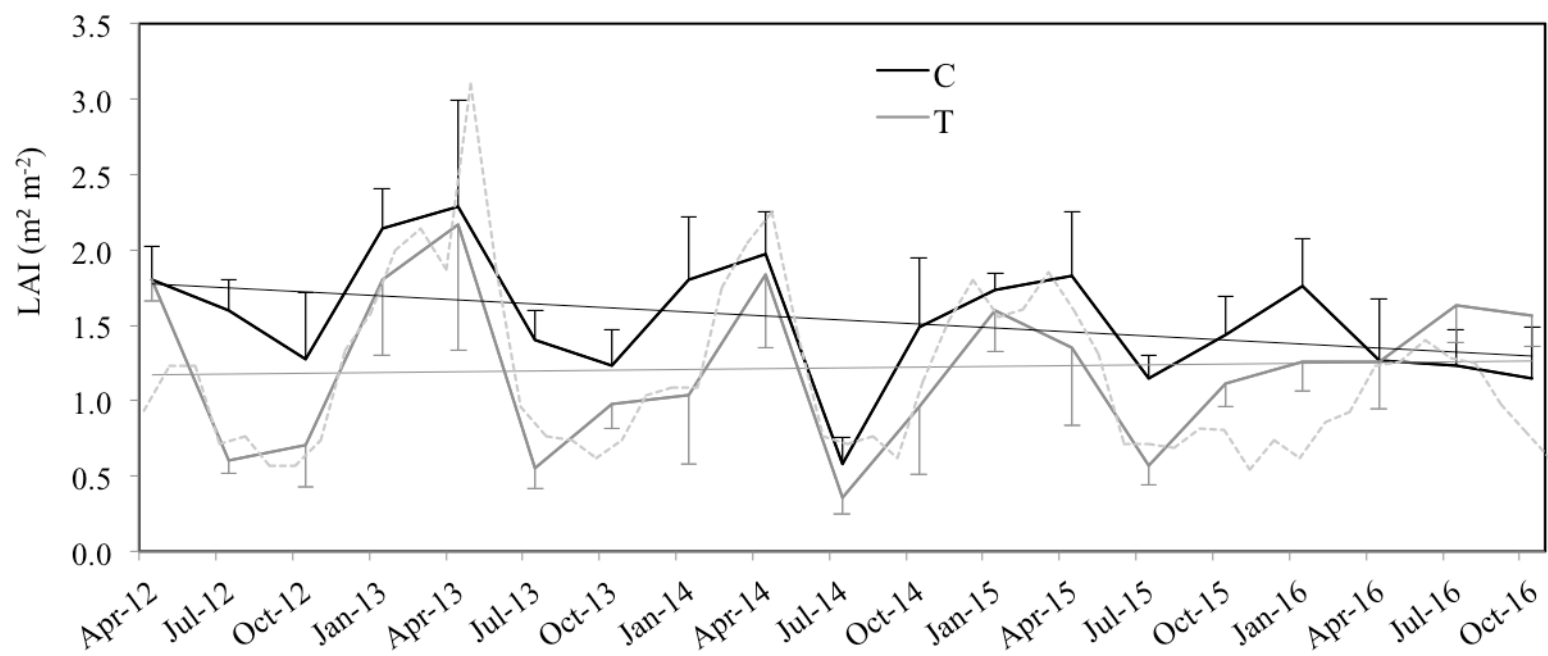


Figure 3



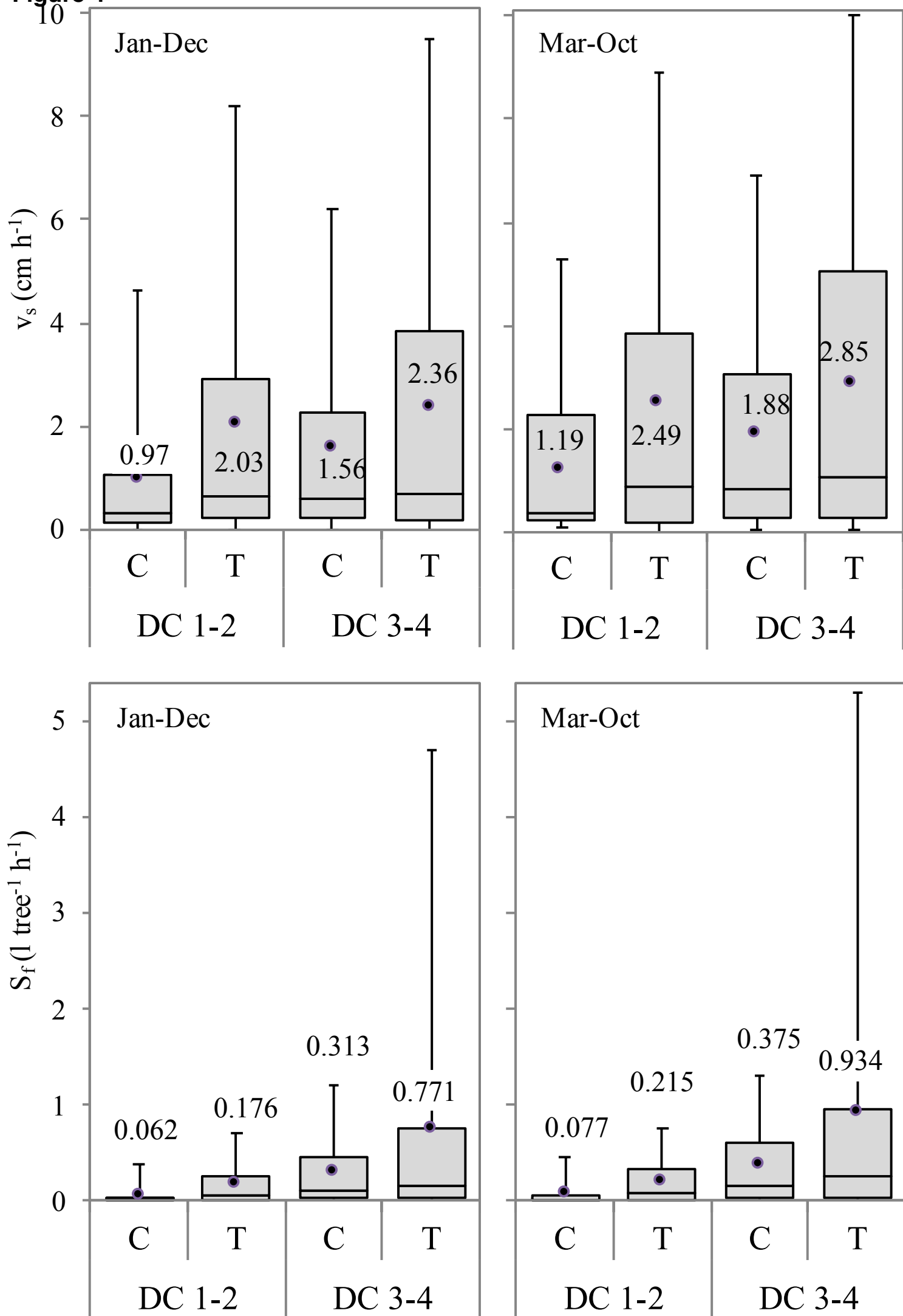
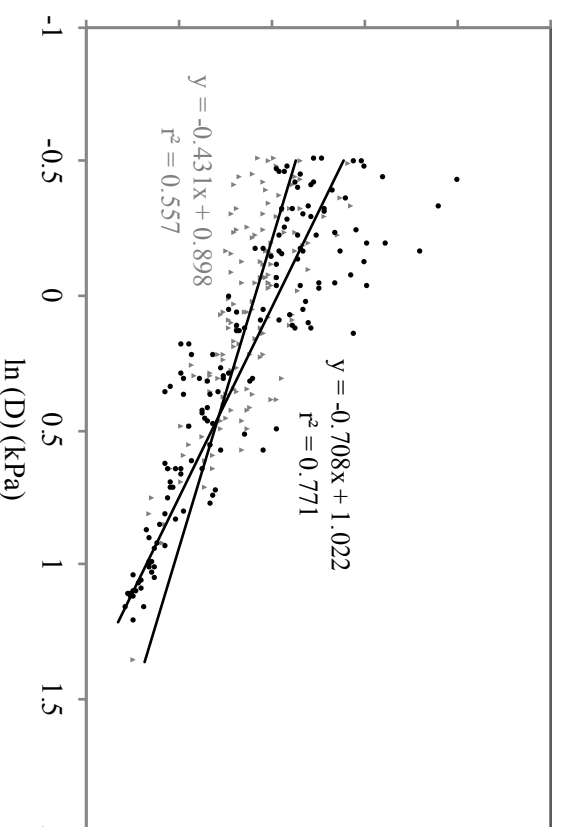
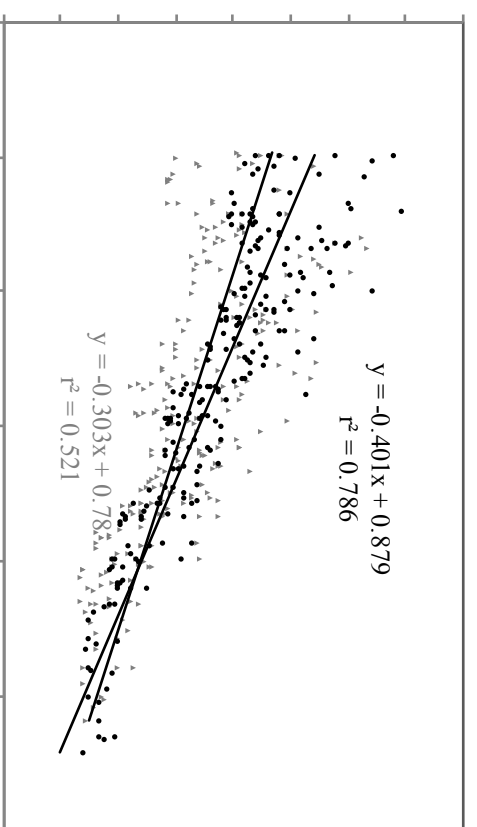
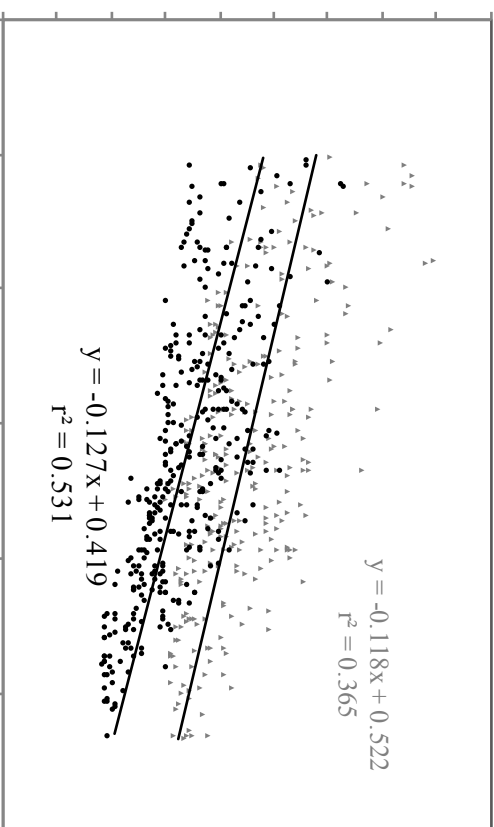
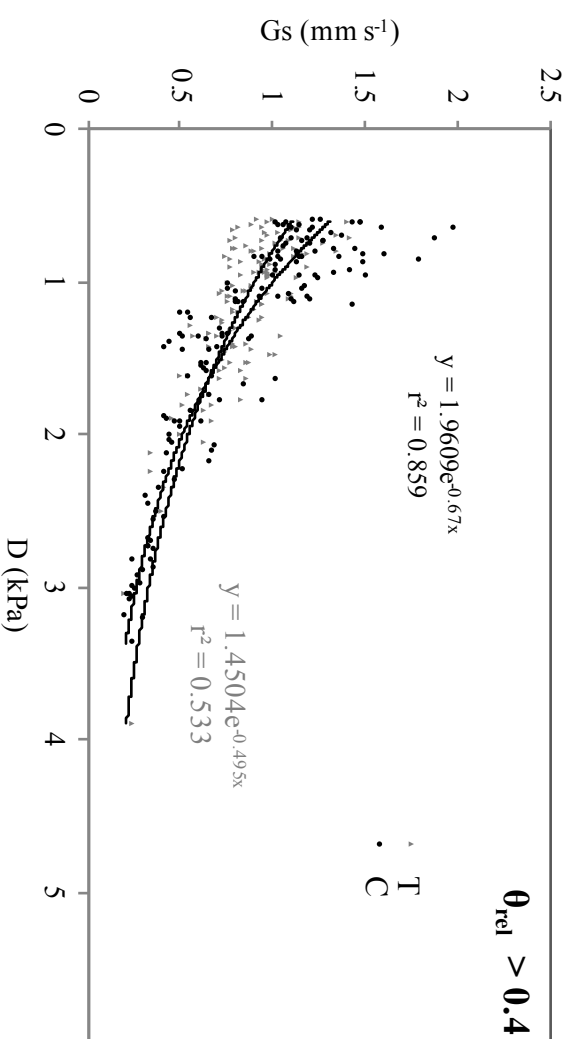
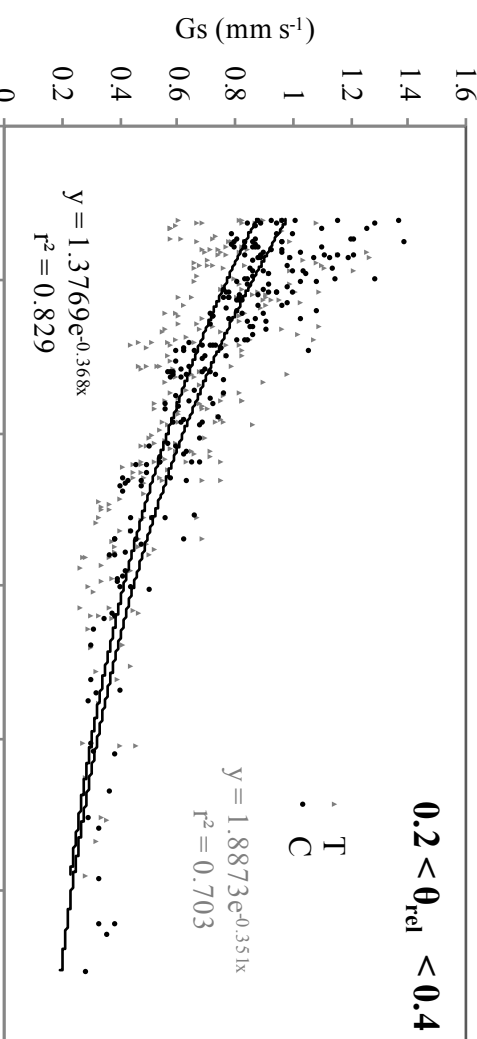
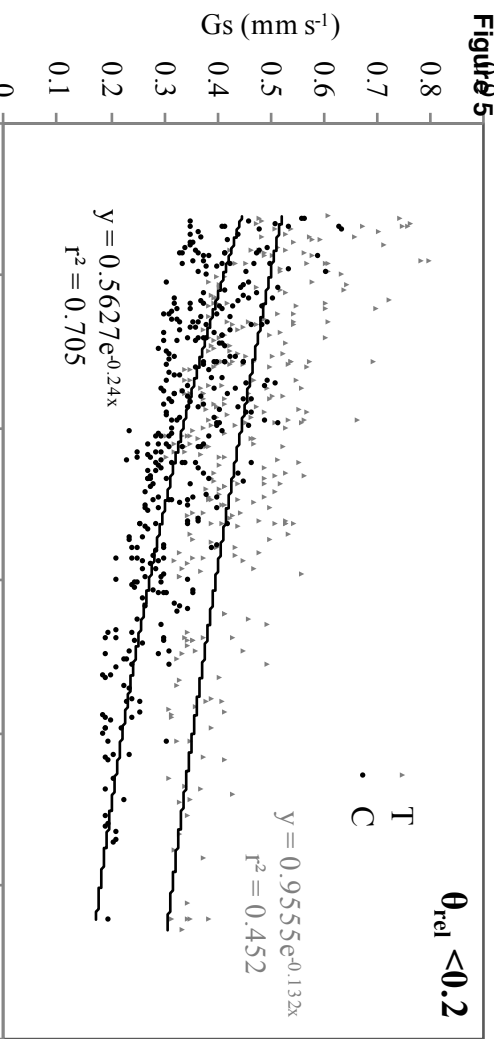
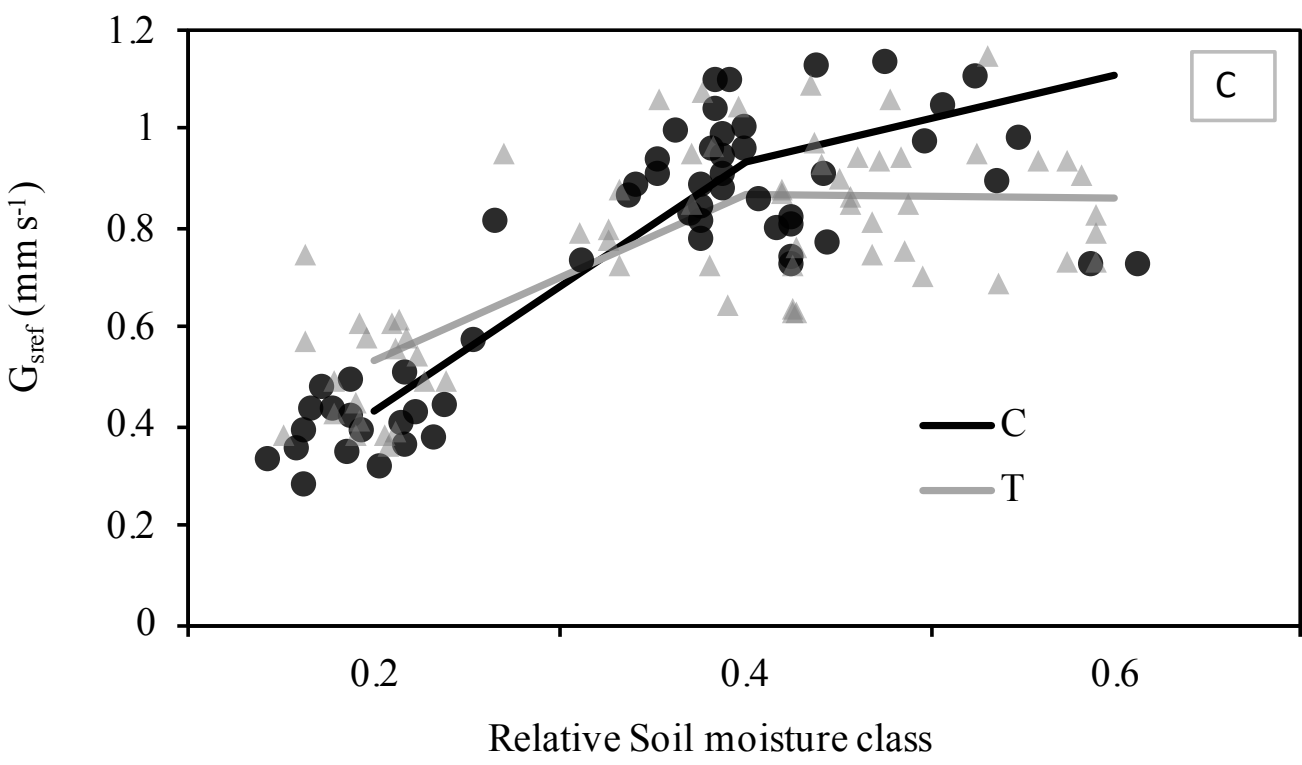
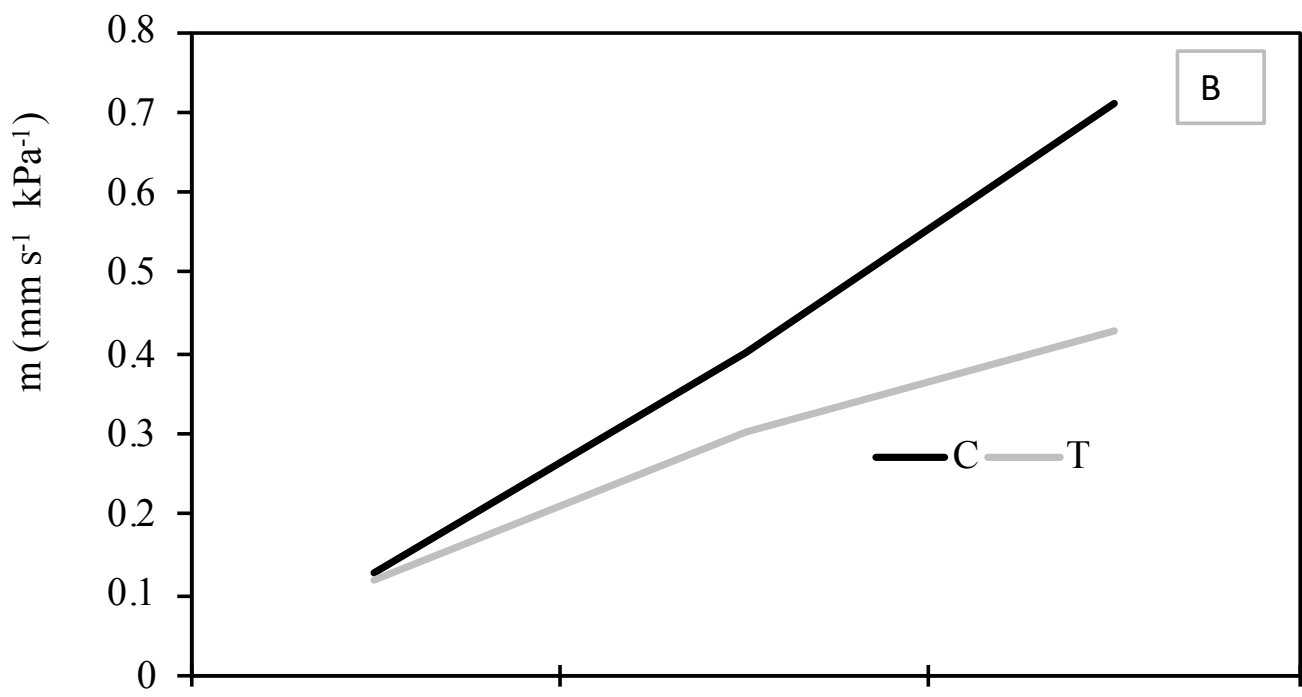
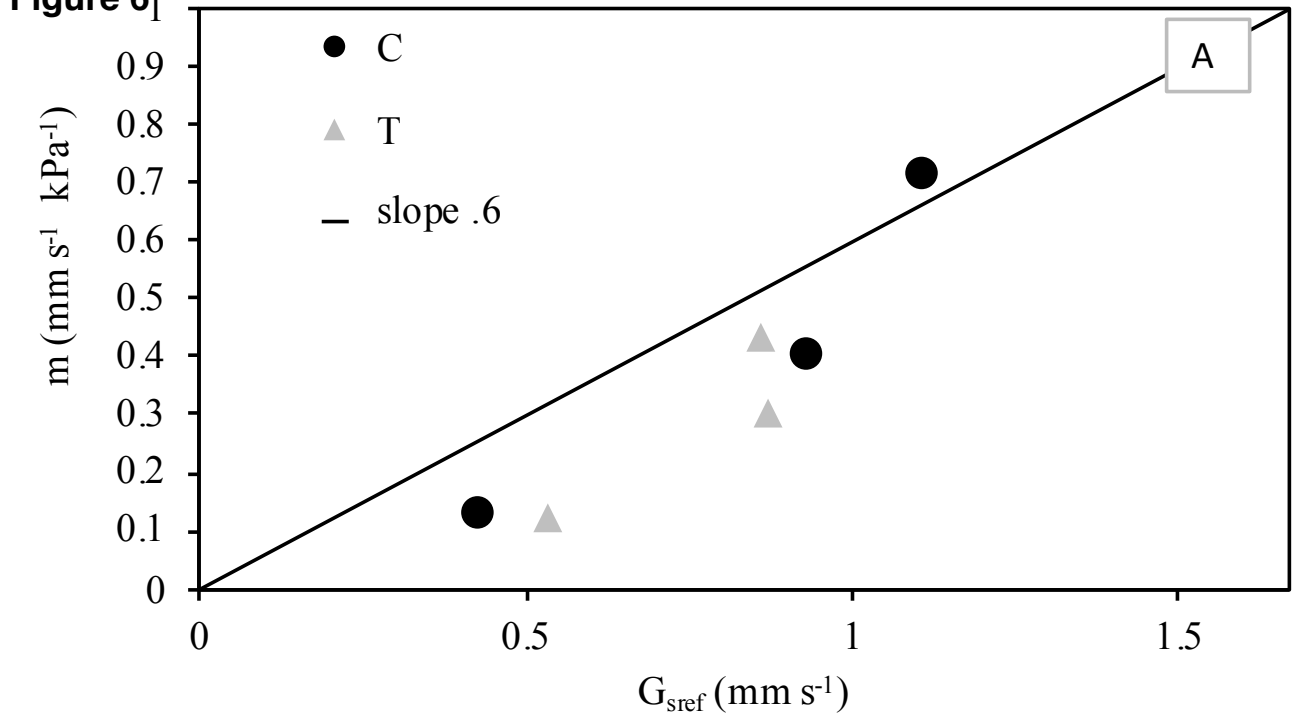
**Figure 4**

Figure 5



**Figure 6**



Jan-Dec

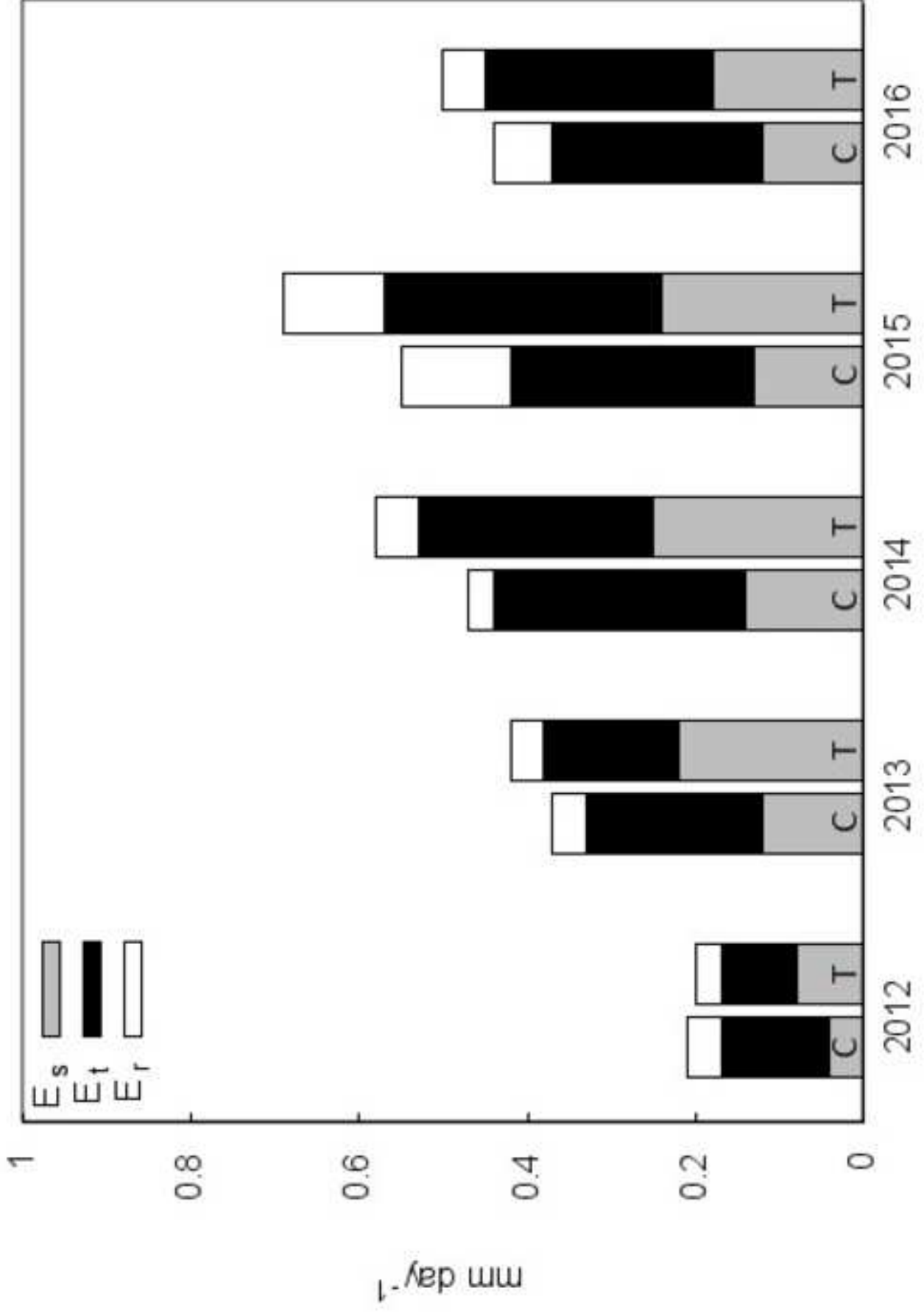


Figure 7a  
[Click here to download high resolution image](#)

Mar-Oct

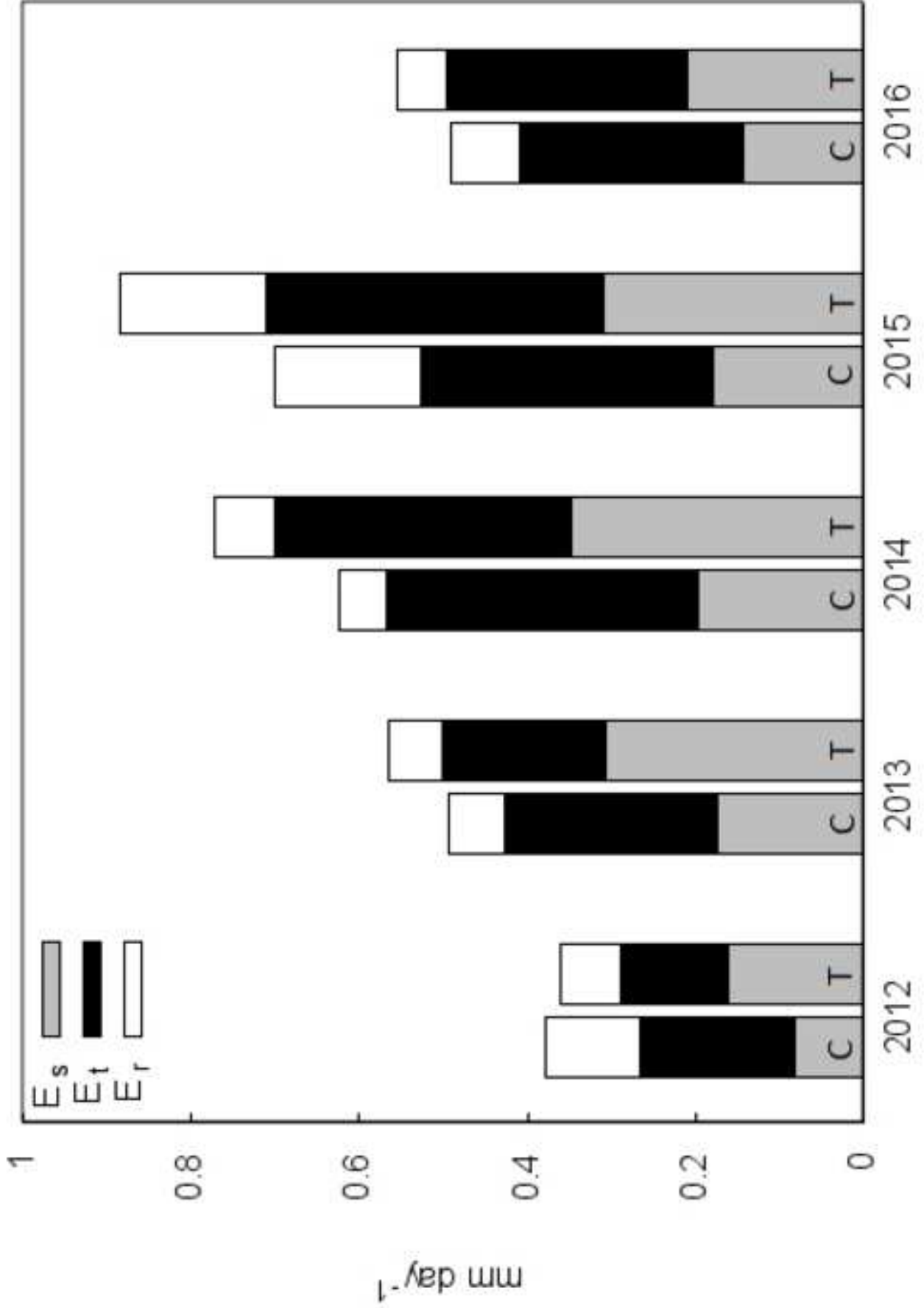


Figure 7b  
[Click here to download high resolution image](#)

Figure 8

